THE ASTROPHYSICAL JOURNAL SUPPLEMENT SERIES, 125:363–407, 1999 December

A SUBARCSECOND-RESOLUTION NEAR-INFRARED STUDY OF SEYFERT AND "NORMAL" GALAXIES. I. IMAGING DATA

REYNIER F. PELETIER,[1] JOHAN H. KNAPEN,[2,3] ISAAC SHLOSMAN,[4] D. PÉREZ-RAMÍREZ,[2] D. NADEAU,[3,5] R. DOYON,[3,5] J. M. RODRIGUEZ ESPINOSA,[6] AND A. M. PÉREZ GARCÍA[6]

Received 1999 April 6; accepted 1999 June 8

ABSTRACT

We present new high-resolution near-infrared observations in the J, H, and K bands, obtained to study the properties of Seyfert host galaxies. The data set consists of images in the three bands of practically the entire CfA sample of Seyfert galaxies, and K-band images of a control sample of nonactive, "normal," galaxies, matched to the Seyfert sample in the distribution of type and inclination. The spatial resolution and sampling of the new images is a factor of 2 better than previously published K-band data. In this paper, we present the data in the form of profiles of surface brightness and color, ellipticity and major axis position angle, as well as gray-scale maps of surface brightness in H or K and both $J-H$ and $H-K$ colors. We compare our surface brightness and color profiles with the literature and find good agreement. Our data are discussed in detail in three subsequent publications, where we analyze the morphologies of Seyfert and normal hosts, quantify the strength of nonaxisymmetric features in disks and their relationship to nuclear activity, address the question of bar fraction in Seyferts and normal galaxies, and analyze the color information in the framework of emission mechanisms in Seyfert 1's and 2's and in nonactive galaxies.

Subject headings: galaxies: photometry — galaxies: Seyfert — galaxies: structure — infrared: galaxies — surveys

1. INTRODUCTION

By studying the relationship between active galactic nuclei (AGNs) and their host galaxies we can learn about the processes that fuel the central activity and the role the AGNs play in galactic evolution. Because high spatial resolution is required for this purpose, the use of nearby samples is most promising.

In the last two decades a number of works have been dedicated to this issue. Early optical surveys (Adams 1977; Heckman 1978; Simkin, Su, & Schwarz 1980; Dahari 1984) studied the fraction of bars in Seyfert galaxies, to find the link between Seyfert nuclear activity and nonaxisymmetric distortions of the gravitational potentials of host galaxies by large-scale stellar bars and tidal interactions. This view was supported by theoretical arguments that gravitational torques are able to remove the excess angular momentum from inflowing gas, leading to central or nuclear activity (e.g., reviews by Athanassoula 1996 and Phinney 1994). However, the early observational results were questioned because the control samples were not matched to the Seyfert sample in such important properties like morphological distribution (Balick & Heckman 1982; Fuentes-Williams & Stocke 1988; Shlosman, Begelman, & Frank 1990). Furthermore, it has been shown that a combination of dust obscuration, stellar populations and inadequate spatial resolution can hide even a strong bar in the optical (e.g., Thronson et al. 1989; Block & Wainscoat 1991; Spillar et al. 1992).

It is clear that in the near-infrared (NIR), where one can look through the dust, more bars are found (McLeod & Rieke 1995), but the fact that NIR arrays until recently covered small areas on the sky made galaxy classification in the NIR a very tedious job. Even very recent studies (e.g., Moles, Márquez, & Pérez 1995; Ho, Filippenko, & Sargent 1996) had to rely on the morphological classification from optical catalogs (e.g., de Vaucouleurs et al. 1991, hereafter RC3). Only Mulchaey & Regan (1997), using K-band observations with a field size of about $3' \times 3'$, do not take this route and conclude from NIR observations of Seyfert and control galaxies that the bar fractions are equal in these two classes.

Apart from studying the morphology, one can also make use of optical and NIR colors to investigate the nature of Seyfert galaxies. Traditionally, Seyfert galaxies are classified into two categories, i.e., the Seyfert 1's with broad, and the Seyfert 2's with narrow emission lines. The "unified model for AGNs" explains the observed differences between the two classes of Seyferts in terms of orientation effects with respect to the observer (see Antonucci 1993 for a review). The model invokes an optically thick torus, which surrounds the region responsible for the production of the broad lines (BLR) and is oriented edge-on for Seyfert 2's, and face-on for Seyfert 1's. The main observational support for this scheme comes from spectropolarimetry, showing scattered light from the BLR in Seyfert 2 galaxies, and from striking biconical structures in line emission maps (e.g., NGC 5252; Tadhunter & Tsvetanov 1989). NIR colors are generally well fitted by a combination of stellar populations and hot dust of about 1000–1300 K (e.g., Glass & Moorwood 1985; Alonso-Herrero et al. 1998). Infrared color-

[1] Department of Physics, University of Durham, South Road, Durham, DH1 3LE, UK: R.F.Peletier@dur.ac.uk.

[2] Department of Physical Sciences, University of Hertfordshire, Hatfield, Herts AL10 9AB, UK; knapen@star.herts.ac.uk.

[3] Visiting Astronomer, Canada-France-Hawaii Telescope operated by the National Research Council of Canada, the Centre National de la Recherche Scientifique de France and the University of Hawaii.

[4] Department of Physics and Astronomy, University of Kentucky, Lexington, KY 40506-0055; shlosman@pa.uky.edu.

[5] Observatoire du Mont Mégantic and Département de Physique, Université de Montréal, C. P. 6128, Succursale Centre Ville, Montréal, Québec, H3C 3J7, Canada; nadeau@astro.umontreal.ca, doyon@astro.umontreal.ca.

[6] Instituto de Astrofísica de Canarias, E-38200 La Laguna, Tenerife, Spain; jre@iac.es, apg@iac.es.

TABLE 1

PROPERTIES OF OUR SEYFERT SAMPLE GALAXIES

Galaxy (1)	Seyfert (2)	Type (3)	R.A. (4)	Decl. (5)	z (6)	M_K (7)	M_B (8)	MGT (9)
Mrk 334	1.8	.P.....	00 03 09.622	+21 57 36.56	0.0220	−23.8	−20.1	RS1
Mrk 335	1	.P.....	00 06 19.519	+20 12 10.49	0.0259	−24.2	−20.7	SS1
UGC 524	1	PSBS3..	00 51 35.010	+29 24 04.53	0.0359	−24.7	−21.3	
1 Zw 1	1	.S?....	00 53 34.940	+12 41 36.20	0.0604	−24.4	−22.4	
Mrk 993	2	.S..1..	01 25 31.464	+32 08 11.43	0.0154	−23.6	−19.4	RS2
Mrk 573	2	RLXT+*.	01 43 57.802	+02 20 59.65	0.0173	−23.8	−19.5	RS2
UGC 1395	1.9	.SAT3..	01 55 22.039	+06 36 42.65	0.0174	−23.7	−19.9	
Mrk 590	1.2	.SAS1*.	02 14 33.562	−00 46 00.09	0.0263	−24.8	−20.5	SS1
NGC 1068	2	RSAT3..	02 42 40.711	−00 00 47.81	0.0037	−24.7	−19.3	
NGC 1144	2	.RING. B	02 55 12.196	−00 11 00.81	0.0288	−25.5	−19.8	RS2
Mrk 1243	1	.S..1..	09 59 55.835	+13 02 37.76	0.0353	−24.1	−19.9	
NGC 3227	1.5	.SXS1P.	10 23 30.589	+19 51 53.99	0.0038	−23.8	−16.5	SS1
NGC 3362	2	.SX.5..	10 44 51.716	+06 35 48.24	0.0227	−24.7	−21.6	RS2
UGC 6100	2	.S..1?.	11 01 33.999	+45 39 14.16	0.0291	−24.2	−20.9	RS2
NGC 3516	1.5	RLBS0*.	11 06 47.490	+72 34 06.88	0.0085	−23.6	−19.3	SS1
Mrk 744	1.8	.SXT1P.	11 39 42.551	+31 54 33.43	0.0091	−22.3	−18.1	SS1
NGC 3982	2	.SXR3*.	11 56 28.102	+55 07 30.58	0.003	−21.9	−19.1	RS2
NGC 4051	1	.SXT4..	12 03 09.614	+44 31 52.80	0.0022	−23.3	−16.2	SS1
NGC 4151	1.5	PSXT2*.	12 10 32.579	+39 24 20.63	0.0030	−23.9	−18.3	
NGC 4235	1	.SAS1./	12 17 09.904	+07 11 29.08	0.0077	−23.8	−19.0	RS1
Mrk 766	1.5	PSBS1*.	12 18 26.509	+29 48 46.34	0.0128	−23.3	−19.1	SS1
Mrk 205	1	.P.....	12 21 44.120	+75 18 38.25	0.070	−24.7	−23.5	
NGC 4388	2	.SAS3*/	12 25 46.701	+12 39 40.92	0.008	−22.5	−16.9	
NGC 4395	1.8	.SAS9*.	12 25 48.918	+33 32 48.43	0.0011	−21.6	−14.3	
Mrk 231	1	.SAT5$P	12 56 14.2344	+56 52 25.236	0.0410	−26.3	−21.3	
NGC 5033	1.9	.SAS5..	13 13 27.526	+36 35 38.08	0.0030	−24.4	−18.3	
Mrk 789	1	.P.....	13 32 23.984	+11 06 20.19	0.032	−24.0	−20.7	
UGC 8621	1.8	.S?....	13 37 39.870	+39 09 16.99	0.0201	−23.8	−20.1	
NGC 5252	1.9	.L.....	13 38 15.963	+04 32 33.29	0.0231	−24.6	−19.5	RS1
Mrk 266	2	.P.....	13 38 17.69	+48 16 33.9	0.0275	−23.6	−20.9	RS2
Mrk 270	2	.L...?.	13 41 05.759	+67 40 20.32	0.0090	−22.7	−17.7	RS2
NGC 5273	1.9	.LAS0..	13 42 08.338	+35 39 15.17	0.0036	−21.8	−16.6	
Mrk 461	2	.S.....	13 47 17.745	+34 08 55.34	0.016	−23.1	−19.3	
NGC 5347	2	PSBT2..	13 53 17.834	+33 29 26.98	0.0304	−22.6	−18.9	RS2
Mrk 279	1	.L.....	13 53 03.447	+69 18 29.57	0.036	−24.5	−20.2	
NGC 5548	1.5	PSAS0..	14 17 59.534	+25 08 12.44	0.0166	−24.1	−19.7	SS1
NGC 5674	1.9	.SX.5..	14 33 52.243	+05 27 29.65	0.0248	−24.7	−21.2	RS1
Mrk 817	1.5	.S?....	14 36 22.068	+58 47 39.38	0.0314	−24.7	−21.1	SS1
Mrk 686	2	.SB.3..	14 37 22.123	+36 34 04.11	0.0122	−23.7	−19.1	RS2
Mrk 841	1	.....	15 04 01.201	+10 26 16.15	0.0364	−24.7	−20.5	
NGC 5929	2	.S..2*P	15 26 06.161	+41 40 14.40	0.0083	−22.0	−18.1	RS2
NGC 5940	1	.SB.2..	15 31 18.070	+07 27 27.91	0.0339	−24.8	−20.0	US1
NGC 6104	1.5	.S?....	16 16 30.686	+35 42 29.00	0.0280	−24.3	−20.9	RS1
UGC 12138.....	1.8	.SB.1..	22 40 17.048	+08 03 14.09	0.0250	−23.6	−20.6	US1
NGC 7469	1	PSXT1..	23 03 15.623	+08 52 26.39	0.0160	−25.0	−20.3	SS1
Mrk 530	1.5	.SAT3*P	23 18 56.617	+00 14 38.23	0.0290	−25.3	−20.5	SS1
Mrk 533	2	.SAR4P.	23 27 56.724	+08 46 44.53	0.0289	−25.2	−20.8	SS2
NGC 7682	2	.SBR2..	23 29 03.928	+03 32 00.00	0.0170	−23.9	−19.6	RS2

NOTES.—(Col. [1]) galaxy name; (col. [2]) Seyfert type (from Huchra & Burg 1992); (col. [3]) morphological classification (from RC3); (cols. [4] and [5]) R.A. and Decl. (J2000, from NASA Extragalactic Database NED) (units of right ascension are hours, minutes, and seconds, and units of declination are degrees, arcminutes, and arcseconds); (col. [6]) redshift (NED); (cols. [7] and [8]) absolute magnitude in K and B (from McLeod & Rieke 1995); (col. [9]) Seyfert host galaxy type (from *HST* observations of Malkan et al. 1998).

color diagrams, like the $J-H$ versus $H-K$ diagram, show that the light in near the nuclei of many Seyfert galaxies cannot be reproduced purely by starlight, even extincted by dust, because for a given $J-H$ the $H-K$ is just too red (e.g., Alonso-Herrero et al. 1998). $H-K$ colors larger than 1 are sometimes seen in Seyfert nuclei, which should be compared to the reddest stars, which have $H-K \sim 0.45$ (Bessell & Brett 1988). It is thought that in such a case, a significant fraction of the light comes from thermal radiation from dust heated by a primary ultraviolet source, which could be the AGN or a site of star formation (Rieke 1978). In the case of 3C 273 Barvainis (1987) has shown that he could reproduce its spectrum, with a bump at 2 μm due to emission by ≈ 700 $M_\odot$ of dust of ≈ 1000 K situated between 2 and 20 pc from the nucleus. Others (e.g., Alonso-Herrero et al. 1998) have shown that the position of Seyferts in the $J-H$ versus $H-K$ diagram is well fitted by such models. To see emission from hot dust, one has to go to the K band, since the H

TABLE 2

PROPERTIES OF OUR CONTROL SAMPLE GALAXIES

Galaxy (1)	Type (2)	R.A. (3)	Decl. (4)	z (5)
NGC 1093.....	.SX.2?.	02 48 16.11	+34 25 11.4	0.018
UGC 3247.....	.S?....	05 06 38.1	+08 40 24	0.011
UGC 3407.....	.S..1..	06 09 08.081	+42 05 05.85	0.012
UGC 3463.....	.SXS4..	06 26 55.18	+59 04 41.1	0.009
UGC 3536.....	.L.....	06 46 03.74	+29 20 52.7	0.016
UGC 3576.....	.SBS3..	06 53 06.96	+50 02 02.0	0.020
UGC 3592.....	RSBS1..	065513.83	+40 20 16.2	0.044
NGC 2347.....	PSAR3*.	07 16 04.35	+64 42 36.4	0.015
UGC 3789.....	RSAR2..	07 19 31.53	+59 21 21.1	0.011
NGC 2365.....	.SX.1..	07 22 22.33	+22 05 00.6	0.008
UGC 3850.....	PSXS1..	07 28 14.97	+63 15 21.0	0.016
NGC 2431.....	PSBS1*.	07 45 13.393	+53 04 30.39	0.019
NGC 2460.....	.SAS1..	07 56 52.77	+60 21 00.0	0.005
NGC 2487.....	.SB.3..	07 58 20.10	+25 08 59.0	0.008
NGC 2599.....	.SA.1..	08 32 11.20	+22 33 37.4	0.016
NGC 2855.....	RSAT0..	09 21 27.28	−11 54 35.5	0.006
NGC 3066.....	PSXS4P.	10 02 11.071	+72 07 31.43	0.007
NGC 3188.....	RSBR2..	10 19 42.75	+57 25 24.5	0.026
NGC 3455.....	PSXT3..	10 54 31.37	+17 17 08.2	0.004
NGC 4146.....	RSXS2..	12 10 18.44	+26 25 53.7	0.022
NGC 4369.....	RSAT1..	12 24 36.18	+39 22 58.2	0.003
NGC 4956.....	.L.....	13 05 00.91	+35 10 40.6	0.016
NGC 4966.....	.S.....	13 06 17.20	+29 03 47.2	0.023
NGC 5434.....	.SA.5..	14 03 23.11	+09 26 51.5	0.019
NGC 5534.....	PSXS2P*	14 17 40.57	−07 25 01.1	0.009
NGC 5832.....	.SBT3$.	145 74 5.34	+71 40 55.3	0.001
NGC 5869.....	.L..0*.	15 09 49.29	+00 28 13.2	0.007
UGC 9965.....	.SAT5..	15 40 06.79	+20 40 52.7	0.014
NGC 5992.....	.S.....	15 44 21.457	+41 05 07.85	0.032
NGC 6085.....	.S..1..	16 12 35.225	+29 21 54.16	0.034
NGC 6278.....	.L.....	17 00 50.13	+23 00 40.7	0.009
NGC 6504.....	.S.....	17 56 05.836	+33 12 29.99	0.016
NGC 6635.....	.L...P*	18 27 37.04	+14 49 06.6	0.017
NGC 6922.....	.SAT5P*	20 29 52.90	−02 11 23.8	0.019

NOTES.—Columns are as in Table 1: (col. [1]) name; (col. [2]) morphological classification; (cols. [3] and [4]) R.A. and Decl. (units of right ascension are hours, minutes, and seconds, and units of declination are degrees, arcminutes, and arcseconds); (col. [6]) redshift.

band is generally barely affected. Seyfert galaxies, in addition to hot dust, must also contain a large amount of cold dust, causing the optical BLR to be completely obscured in Seyfert 2's. This cold dust will extinguish and redden the colors of the nucleus. High-resolution NIR color profiles will provide information about the extent of the region containing hot dust, and in this way will constrain both the energy radiated by the central engine and the kinematics of the dusty torus.

This is the first in a series of four papers in which we study the morphology and photometry of Seyfert galaxies, and compare them with nonactive ("normal") galaxies. For this purpose, we have observed the CfA sample, an unbiased sample of Seyfert 1's and 2's (Huchra & Burg 1992) in the J, H, and K bands with a median seeing of 0".7, i.e., more than a factor of 2 better than in previous NIR surveys (McLeod & Rieke 1995; Hunt et al. 1997; Mulchaey, Regan, & Kundu 1997; Hunt et al. 1999). This data set is presented along with imaging of a control sample of nonactive galaxies, matched to the CfA sample. To compensate for the fact that our field size is only about 1', we have combined our data in the outer parts of the galaxies with ellipticity and position profiles obtained from the Palomar Sky Survey (Lasker et al. 1990). Since in the outer parts of spirals the influence of extinction is much less than near the center (e.g., Peletier et al. 1995), this will most likely give results similar to those from large-size NIR arrays. Here (Paper I), we describe the observations of the CfA and control samples and present the imaging data, accompanied by fits to the NIR & POSS images. Knapen, Shlosman, & Peletier (1999, hereafter Paper II) compare both samples to analyze the prevailing morphologies of Seyfert and normal hosts and their bar fractions. Shlosman, Peletier, & Knapen (1999, hereafter Paper III) address the issue of bar strengths in Seyfert and non-Seyfert galaxies.

This paper is organized as follows. In § 2, we describe the samples and in § 3 the observations. In § 4, the data reduction steps are discussed, and in § 5 we compare our observations with previous work in the literature. A summary is given in § 6. Finally, the Appendix gives some notes on the individual objects.

2. SAMPLES

The Seyfert sample considered here is the CfA sample (Huchra & Burg 1992). It is basically a spectroscopically

TABLE 3

DATES OF OBSERVING RUN, TELESCOPE USED, AND SEEING VALUES IN EACH BAND, FOR THE Sy SAMPLE

GALAXY	OBSERVING RUN	SEEING (arcsec)		
		J	*H*	*K*
Mrk 334	1995 Sep/WHT	1.04	1.12	0.74
Mrk 335	1995 Sep/WHT	1.27	1.09	0.75
UGC 524	1995 Sep/WHT	0.72	0.91	0.80
I Zw 1.....	1995 Sep/WHT	0.77	0.75	0.79
Mrk 993	1995 Sep/WHT	0.81	0.74	0.69
Mrk 573	1995 Sep/WHT	0.81	0.77	0.80
UGC 1395	1995 Sep/WHT	0.86	0.74	0.74
Mrk 590	1995 Sep/WHT	0.99	0.78	0.87
NGC 1068	1995 Sep/WHT	0.95	0.82	0.69
NGC 1144	1995 Sep/WHT	0.89	0.81	0.77
Mrk 1243	1996 Feb/CFHT	0.71	0.75	0.76
NGC 3227	1996 Apr/WHT	0.73	0.68	0.62
NGC 3362	1996 Apr/WHT	0.59	0.69	0.75
UGC 6100	1996 Apr/WHT	0.99	0.94	0.91
NGC 3516	1996 Feb/CFHT	0.71	0.73	0.72
Mrk 744	1996 Feb/CFHT	0.98	1.09	0.81
NGC 3982	1996 Feb/CFHT	0.73	0.73	0.73
NGC 4051	1996 Feb/CFHT	0.73	0.73	0.73
NGC 4151	1996 Apr/WHT	0.62	0.61	0.61
NGC 4235	1996 Feb/CFHT	0.99	1.27	0.95
Mrk 766	1996 Feb/CFHT	1.04	0.93	1.00
Mrk 205	1996 Apr/WHT	0.67	0.69	0.73
NGC 4388	1996 Feb/CFHT	0.77	0.92	0.85
Mrk 231	1996 Feb/CFHT	0.99	0.99	1.03
NGC 5033	1996 Feb/CFHT	1.00	0.75	0.87
Mrk 789	1996 Apr/WHT	0.71	0.69	0.59
UGC 8621	1996 Apr/WHT	0.77	0.76	0.87
NGC 5252	1996 Apr/WHT	0.64	0.71	0.60
Mrk 266	1996 Apr/WHT	0.70	0.65	0.67
Mrk 270	1996 Apr/WHT	0.70	0.65	0.67
NGC 5273	1996 Apr/WHT	0.66	0.83	0.70
Mrk 461	1996 Feb/CFHT	0.90	0.97	0.71
Mrk 279	1996 Apr/WHT	0.73	0.69	0.84
NGC 5548	1996 Apr/WHT	0.66	0.62	0.66
NGC 5674	1996 Apr/WHT	0.74	0.78	0.74
Mrk 817	1995 Sep/WHT	0.89	0.93	0.75
Mrk 686	1995 Sep/WHT	0.76	0.75	0.78
Mrk 841	1995 Sep/WHT	0.92	0.87	0.77
NGC 5929	1995 Sep/WHT	1.43	1.11	0.74
NGC 5940	1995 Sep/WHT	0.83	0.74	0.68
NGC 6104	1995 Sep/WHT	0.75	0.72	0.62
UGC 12138.....	1995 Sep/WHT	0.65	0.70	0.68
NGC 7469	1995 Sep/WHT	0.73	0.75	0.65
Mrk 530	1995 Sep/WHT	0.67	0.70	0.73
Mrk 533	1995 Sep/WHT	0.75	0.70	0.71
NGC 7682	1995 Sep/WHT	1.03	10.2	0.98

TABLE 4

DATES OF OBSERVING RUN, TELESCOPE USED, AND SEEING VALUES IN EACH BAND, FOR THE CONTROL SAMPLE

Galaxy	Observing Run	Seeing *K* (arcsec)
NGC 1093.....	1996 Feb/CFHT	0.94
UGC 3247.....	1996 Feb/CFHT	0.59
UGC 3407.....	1996 Feb/CFHT	0.79
UGC 3463.....	1996 Feb/CFHT	0.85
UGC 3536.....	1996 Feb/CFHT	0.66
UGC 3576.....	1996 Feb/CFHT	0.82
UGC 3592.....	1996 Feb/CFHT	0.81
NGC 2347.....	1996 Feb/CFHT	0.86
UGC 3789.....	1996 Feb/CFHT	0.81
NGC 2365.....	1996 Feb/CFHT	0.74
UGC 3850.....	1996 Feb/CFHT	1.01
NGC 2431.....	1996 Feb/CFHT	1.00
NGC 2460.....	1996 Feb/CFHT	1.04
NGC 2487.....	1996 Feb/CFHT	0.85
NGC 2599.....	1996 Feb/CFHT	0.90
NGC 2855.....	1996 Feb/CFHT	0.80
NGC 3066.....	1996 Feb/CFHT	0.88
NGC 3188.....	1996 Feb/CFHT	1.01
NGC 3455.....	1995 Sep/WHT	...
NGC 4146.....	1995 Sep/WHT	0.71
NGC 4369.....	1995 Sep/WHT	...
NGC 4956.....	1996 Feb/CFHT	0.64
NGC 4966.....	1996 Feb/CFHT	0.60
NGC 5434.....	1995 Sep/WHT	...
NGC 5534.....	1996 Feb/CFHT	0.90
NGC 5832.....	1995 Sep/WHT	0.80
NGC 5869.....	1995 Sep/WHT	0.69
UGC 9965.....	1995 Sep/WHT	0.80
NGC 5992.....	1995 Sep/WHT	0.75
NGC 6085.....	1995 Sep/WHT	0.64
NGC 6278.....	1995 Sep/WHT	0.78
NGC 6504.....	1994 Jun/UKIRT	0.80
NGC 6635.....	1995 Sep/WHT	0.69
NGC 6922.....	1995 Sep/WHT	0.69

selected blue-magnitude–limited sample of active galaxies. We took all galaxies classified by Huchra & Burg (1992) as Seyfert 1's and 2's. The advantage of selecting Seyferts in this way is that it is relatively unbiased, and that one can make comparisons between the properties of Seyferts of types 1 and 2. The sample has been observed at many different wavelengths and is therefore well suited to study the physical properties of AGNs. We excluded 3C 273 because of its large redshift ($z = 0.16$ vs. 0.07, for the second largest). No NIR observations were taken of NGC 4395, since it is a dwarf galaxy, much fainter than the rest of the sample, with such a low surface brightness that we could barely detect the nucleus. NGC 5347 was also not included, for observational reasons. We did observe Mrk 789, which is part of the CfA sample but was not included in the study by McLeod & Rieke (1995). Mrk 471, included by McLeod & Rieke but not by Huchra & Burg, was not included. The sample is shown in Table 1.

We also observed a control sample of 34 galaxies, selected from the RC3 to mimic the Seyfert sample accurately in terms of morphological type (including barred/nonbarred as derived from the RC3 classification) and ellipticity. In Paper II, the detailed selection criteria of this sample are discussed, and the morphology of the galaxies in the two samples compared. The control sample is presented in Table 2.

3. OBSERVATIONS

Observations were performed at the Observatorio del Roque de los Muchachos at La Palma for $\frac{2}{3}$ of the sample, using WHIRCAM (Hughes, Roche, & Dhillon 1996) at the 4.2 m William Herschel Telescope (WHT), and at the 3.6 m

Canada France Hawaii Telescope (CFHT) at Hawaii for the remaining third, using the Montréal NIR camera (MONICA; Nadeau et al. 1994). At La Palma, the observations were made in 1995 September and in 1996 April, whereas all CFHT observations were made in 1996 February. WHIRCAM uses an InSb array with 256 × 256 pixels of 0.″245 on the sky. MONICA uses a 256 × 256 HgCdTe array with a very similar pixel size of 0.″242. To match the ellipticity distribution of the Seyfert and control samples, we added the galaxy NGC 6504 to the control sample. This galaxy had been observed at UKIRT in 1994 using a 256 × 256 InSb array with pixel size of 0.″291 (Peletier & Balcells 1997).

The observing procedure consisted in taking a series of four dithered frames of typically 60 s each, flanked or followed by four dithered sky frames of the same exposure time, taken at offsets of about 5′–10′ from the object. After this, the same procedure was repeated. A small linearity correction was applied to the WHIRCAM data, determined from dome flat fields taken using various integration times. No linearity correction was needed for the CFHT exposures.

Care was taken that none of the exposures were saturated, implying, for example, that the integration time per readout for NGC 4151 in K was 0.5 s. Our exposures for that galaxy, and to a lesser extent for a few others, contain rather strong diffraction spikes, due to the relative strength of the nuclear source. The CFHT exposures suffer to a small extent from residual images. After observing a bright source, the next image may contain a faint point source at the position of the previous peak. The strength of these residual sources was 0.2% of the initial source at most and was only visible for galaxies with very bright nuclei. This hysteresis effect does not affect the data presented here.

For the control sample, K-band images of the same quality as those of the Seyfert sample were obtained. The control sample was observed during the same nights as the Seyfert sample, so the photometric and seeing conditions are the same for both samples.

During the observations some high clouds were present. Comparison with the surface photometry of McLeod & Rieke (1995) and aperture photometry in the literature shows that the attenuation by clouds in J, H, and K in general varied between 0 and 0.5 mag.

To estimate the quality of the images, we have measured the seeing for every galaxy in each band using stars on the galaxy frame or on adjacent sky frames. In some cases no stars were available, and seeing values have been taken from galaxy frames observed approximately at the same time at similar air mass values. The measured values for the FWHM of the images have been given in Tables 3 and 4. They should be considered upper limits for the seeing, given the fact that some images are almost critically sampled. The seeing was generally excellent and varied between 0.″5 and 1.″0. The reduced mosaics have an effective median seeing of about 0.″7.

4. DATA REDUCTION

The basic data reduction procedure was standard, and although different in details for our WHT and CFHT data, can be summarized as follows. After subtracting an appropriate dark frame, all sky frames belonging to a certain object were median combined and subtracted from each object frame. A flat field was created by taking the median of all normalized sky-frames taken during the night. After flat-fielding, a mosaic was made from all object frames by aligning them on the centroid of the nucleus or a bright star. Bad pixels were excluded using a mask. This process is the same as, for example, described in Peletier (1993). Further details of the CFHT data reduction procedure can be found in Pérez-Ramírez et al. (1999, in preparation). The images are shown in Figure 1. The data presented in Figure 1 is tabulated in Tables 5 and 6. Only tabulated are data points for which the error in the H-band surface brightness is less than 1 mag.

During each run, the position angle (from N to E) of the camera was measured by comparing the positions of stars on our frames with images of the POSS Digital Sky Survey. In the same way our pixel size was determined to be 0.″245 $\pm$ 0.005% for the WHIRCAM images, and 0.″242 $\pm$ 0.005% for the MONICA frames. These numbers were used to determine the final radial morphological profiles.

To study the morphology of the galaxies in the Seyfert and Control samples, we fitted ellipses to the images using galphot (see Jørgensen, Franx, & Kjaergaard 1992). We first removed foreground stars by hand and did not consider them in the fit. The center position was allowed to change freely as a function of radius. After ellipse fitting, we determined the residual background sky value for each frame and subtracted it from the profile. This was done by taking a median value of the signal in the outer parts of the frame, which were thought to be the least affected by galaxy emission. For large galaxies a better estimate was made by assuming that the logarithmic slope of the surface brightness profile remained constant outside the frame. Although this might lead to quite large errors, the contribution of most galaxies in the outer parts of the frames is negligible. As an example, for all but the brightest galaxies, the surface brightness in H at the edge of the frame is lower than 21 mag arcsec^{-2}, which is 0.17% of a typical sky surface brightness of 14 mag arcsec^{-2}. Background sky determination error bars are included in Figure 1. One sigma error bars correspond to $\mu_H = 21.5$ mag arcsec^{-2}, $\mu_J = 21.2$ mag arcsec^{-2} and $\mu_K = 20.5$ mag arcsec^{-2}, which corresponds to about 0.1% of the sky background in H and K, and 0.3% in J. The dotted line corresponds to a radius of 1 seeing FWHM, outside which the effects of seeing on the ellipticity and position angle profile in general are small. However, some of our La Palma data suffer from an elongated PSF, as a result of bad tracking of the telescope. In such a case the galaxy images in the inner regions are elongated toward P.A. 90°, and up to a maximum of 2″–3″ these profiles can not be trusted. The effect is present in all frames observed at La Palma and is worst for the most elongated galaxies.

In order to increase the field size, we also took the images of the digitized Palomar Observatory Sky Survey (POSS; E-plates) and fitted ellipses to them in the same way as described above. Although most of these images are saturated in the central regions, they extend further out than would equivalent NIR images, since the POSS images are deep R-band images, and galaxies generally become less dusty when going outward, which implies that they are bluer. One of the reasons that our observations have been taken in the NIR is the fact that spiral galaxies, and especially Seyferts are dusty in general (e.g., Valentijn 1990; Beckman et al. 1996; Alonso-Herrero et al. 1998). However, the amount of extinction generally decreases when going outward. Peletier et al. (1995) showed that the extinction at

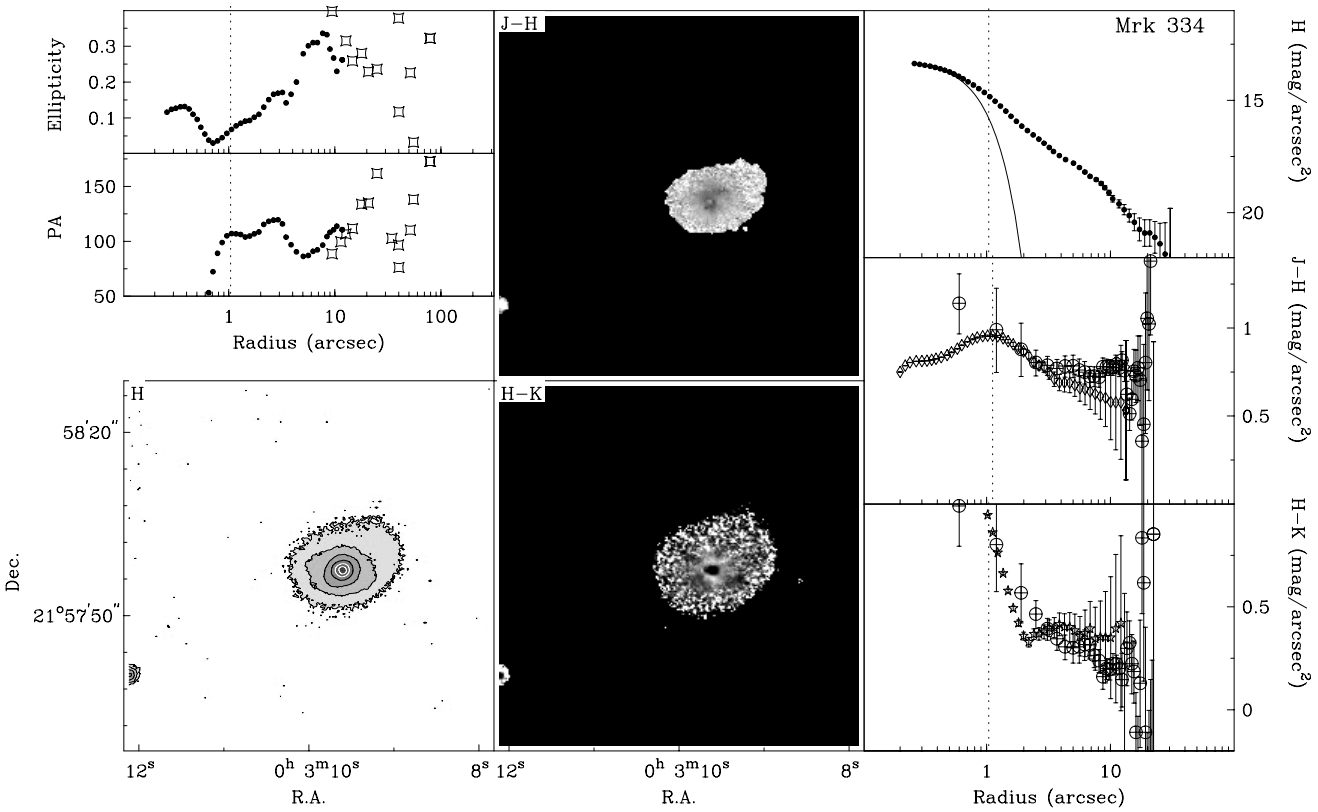

FIG. 1.—Images and photometric profiles for the individual galaxies, also tabulated in Tables 5 and 6. On the upper left ellipticity ($1 - b/a$) and major axis position angle are plotted as a function of major axis radius. The position angle has been measured from N through E. Filled dots are fits to our H-band data, while open squares are fits to the POSS images. The lower right panel is a contour plus gray-scale plot the galaxy. Contours start at $H = 19$ mag arcsec^{-2}, with intervals of 1 mag arcsec^{-2}. For NGC 4395 and NGC 5347, for which POSS data are plotted, the contour zero point is arbitrary, and the contour level 1 mag arcsec^{-2}. The coordinates are J2000.0, obtained from the NASA/IPAC Extragalactic Database (NED). The middle two panels are gray-scale representations of $J-H$ and $H-K$ color index images, with a gray-scale interval of 0.05 mag arcsec^{-2}. The upper right panel show the H-band surface brightness profile (*solid line*) and the PSF at the time of observation (*dashed line*), normalized to the center of the galaxy. The dotted line again indicates 1 seeing FWHM. In the color profiles, lower right panel, the dotted line indicates 1 seeing FWHM of the band with the worst seeing. Open circles indicate the colors of Hunt et al. (1997). For NGC 4395 and NGC 5347 only POSS data have been analyzed and plotted. For the control sample only the surface brightness profile in K, the ellipticity and position angle profile and a gray-scale map of the galaxy are shown (*top to bottom*). The contour levels of the gray-scale map are the same as in K as for the Seyfert galaxies in H. The meaning of the symbols is the same as for the CfA sample.

3 NIR disk scale lengths in B is smaller than 0.5 mag, in general. Our NIR data cover in all cases the inner three scale lengths of our galaxies. Further out, where we have to use the red POSS data, the influence of extinction can be neglected. Agreement between NIR and POSS data sets in the overlap region is generally good. The POSS fits have been plotted along with the NIR fits in Figure 1. In the inner regions no POSS-fit data are shown when those images are saturated.

The observations were all done using partially clouded weather conditions, with high cirrus clouds present on many of the observing nights. In particular, the nights of 1995 September 11 and 12 suffered from clouds. Many of the galaxies observed on those nights were reobserved on September 13. The weather conditions in 1996 February and April were better, with less cirrus. Since on 1996 April 28 the seeing was bad, all observations taken on that day were repeated later. Because of the clouds, the Seyfert data were all photometrically calibrated using aperture photometry in the literature. This is not an ideal situation, since many of these AGNs are variable (e.g., Peterson et al. 1998). We could, however, find aperture photometry in J, H, and K for all but two of the galaxies, Mark 590 and UGC 6100, which we calibrated using standard stars observed during the night. Most of the literature aperture photometry was obtained from Edelson, Malkan, & Rieke (1987; 26 galaxies). Other comparison sources included Spinoglio et al. (1995; 11), Rieke (1978; 4), Rudy et al. (1982; 2) and McAlary (1982; 1). As a check, we compared our K-band data with the surface photometry of McLeod & Rieke (1995). In general the agreement was reasonable. For NGC 5940, however, using photometry of Edelson et al. (1987) there was more than a magnitude difference between the two calibrations, and for that reason we applied our standard star calibration. We claim that the absolute accuracy of our photometry is about 0.3 mag (1 σ rms), based on the comparison with McLeod & Rieke (1995). We refer the reader to § 5 for further details on comparison with the literature.

For the control sample, we used standard stars. On each night in periods without much cloud cover many standard stars were observed from the list of Casali & Hawarden (see Hughes et al. 1996) and Carter & Meadows (1995). For each run, the same photometric calibration was used, and no corrections were applied for atmospheric and galactic extinction, nor were any color terms applied. Comparison with the Seyfert galaxy data, which was photometrically calibrated using aperture photometry in the literature,

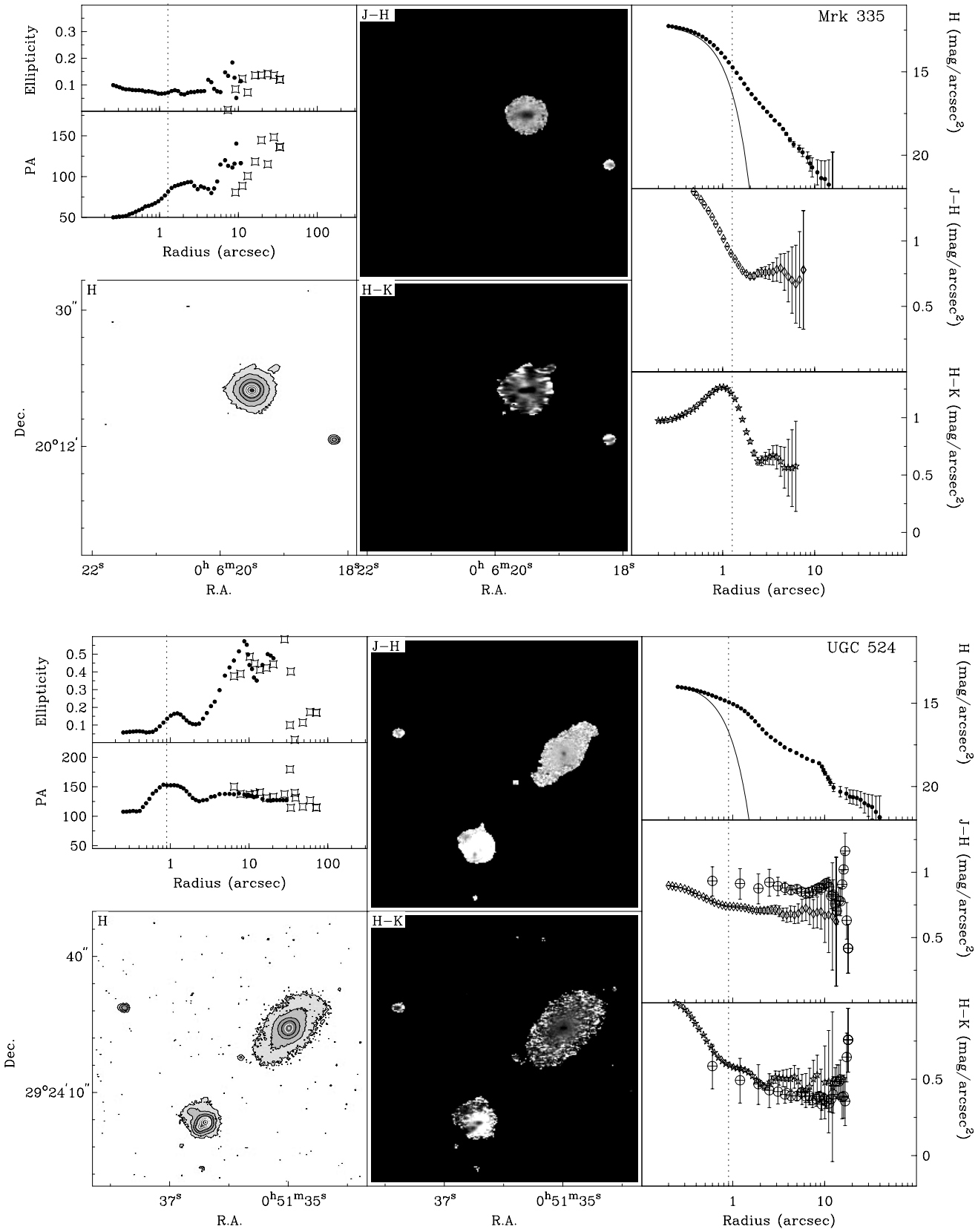

FIG. 1.—*Continued*

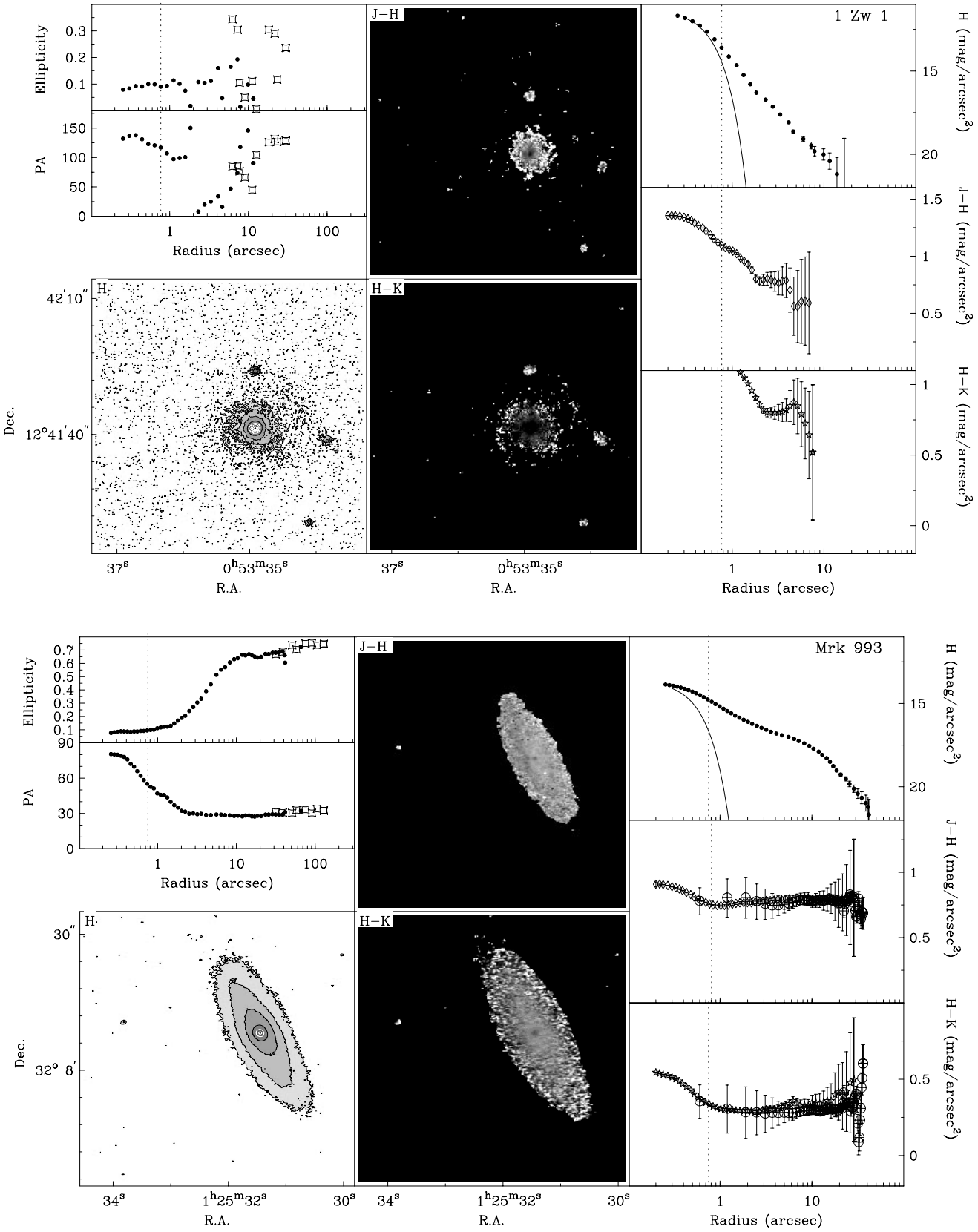

FIG. 1.—*Continued*

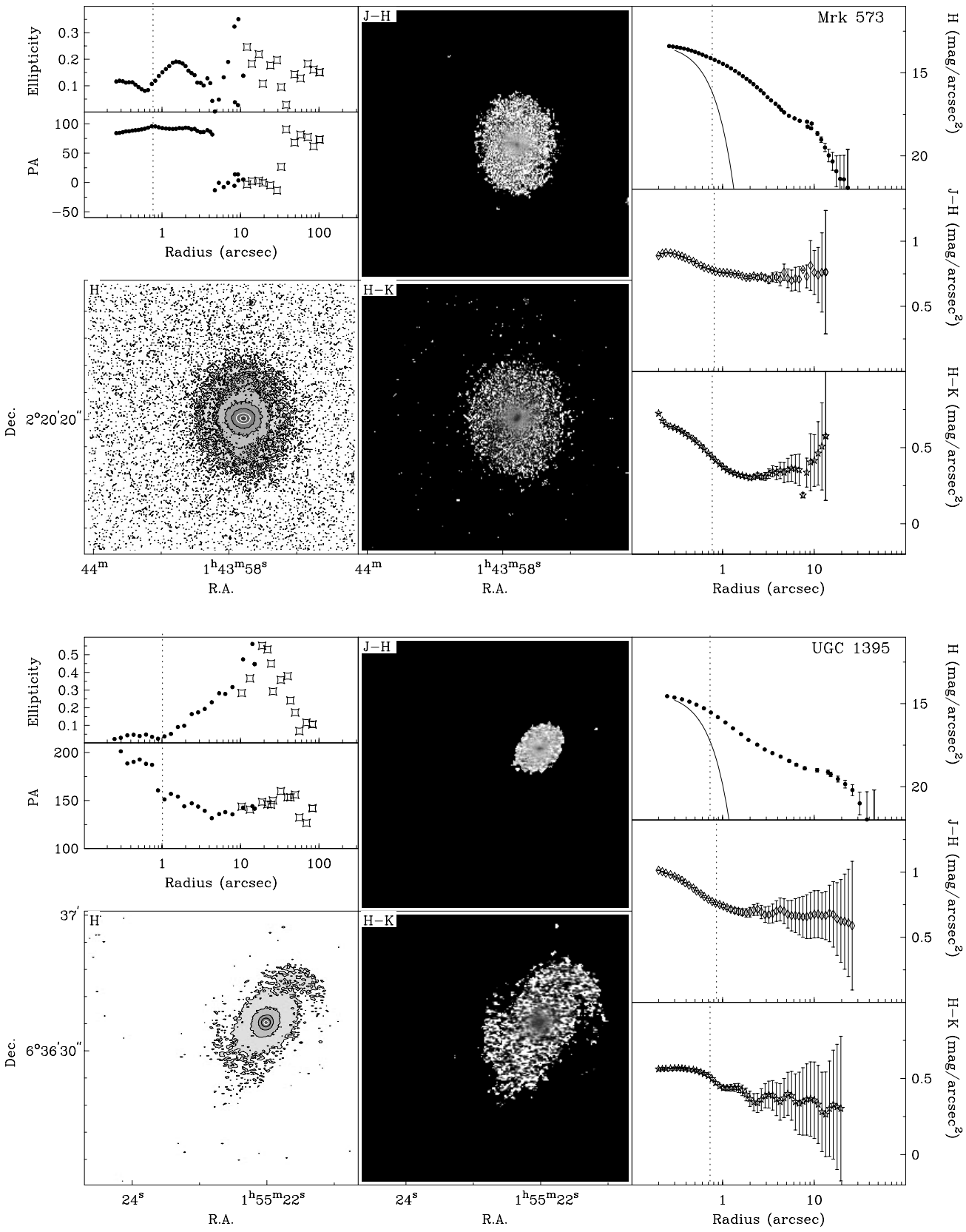

FIG. 1.—*Continued*

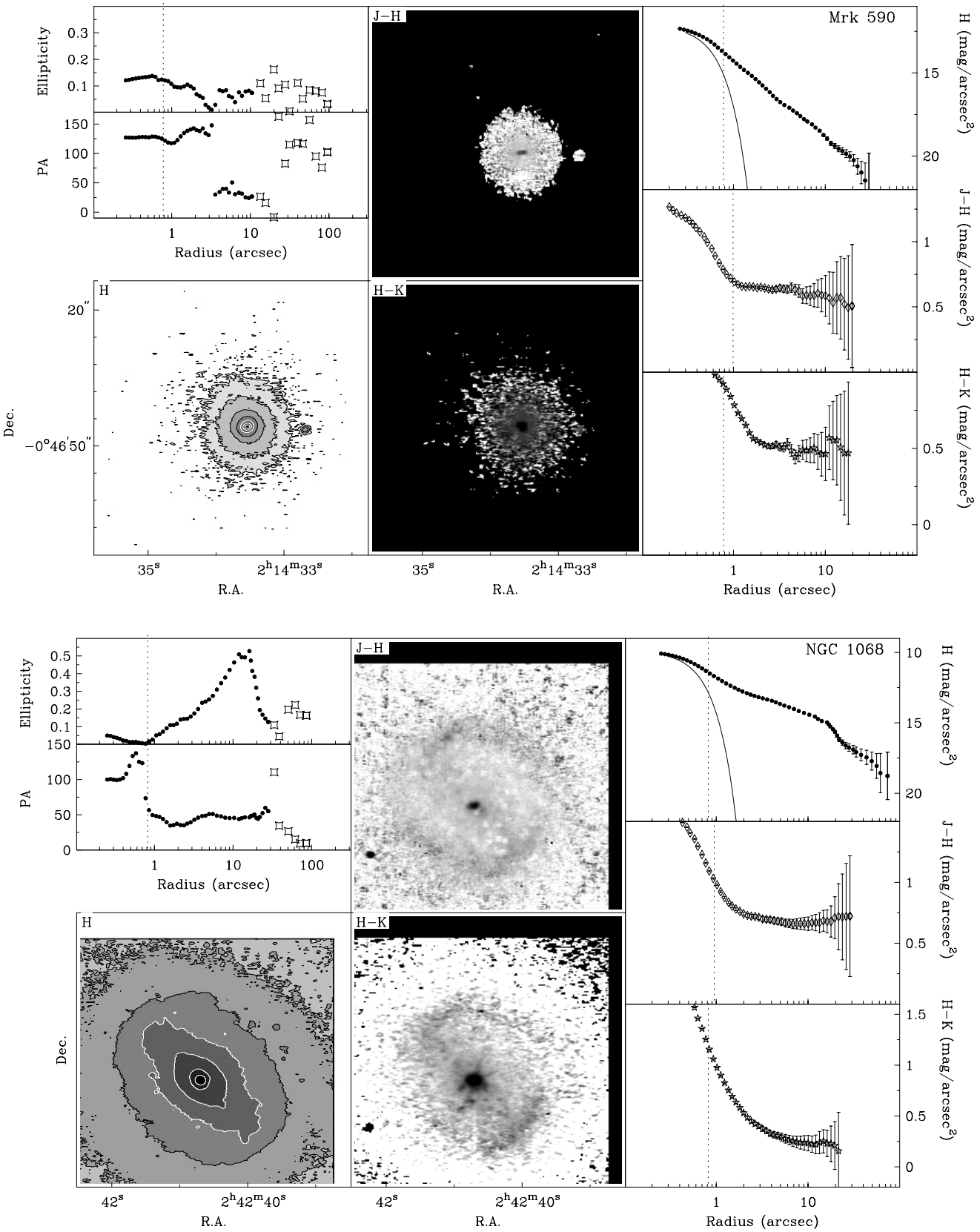

FIG. 1.—*Continued*

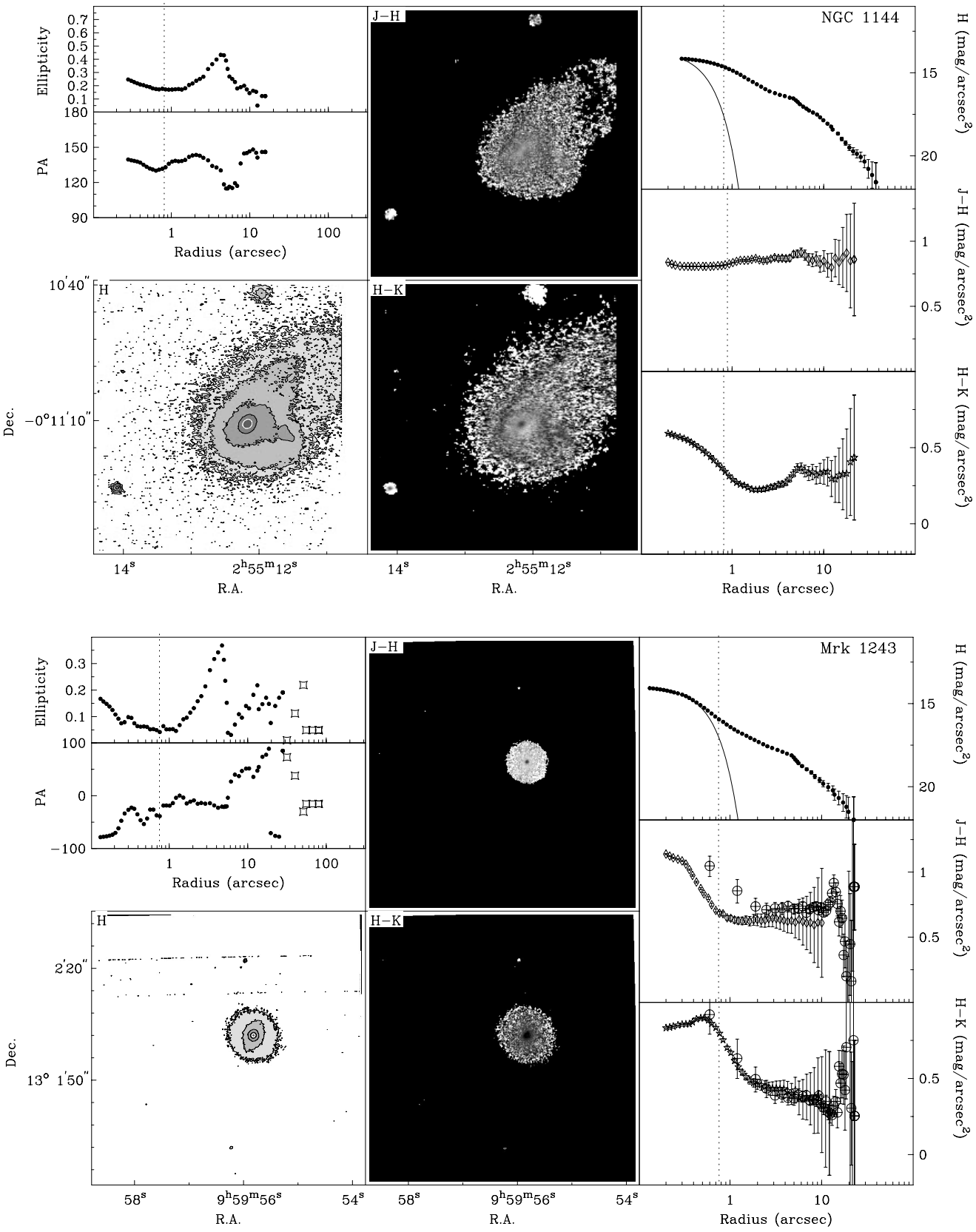

FIG. 1.—*Continued*

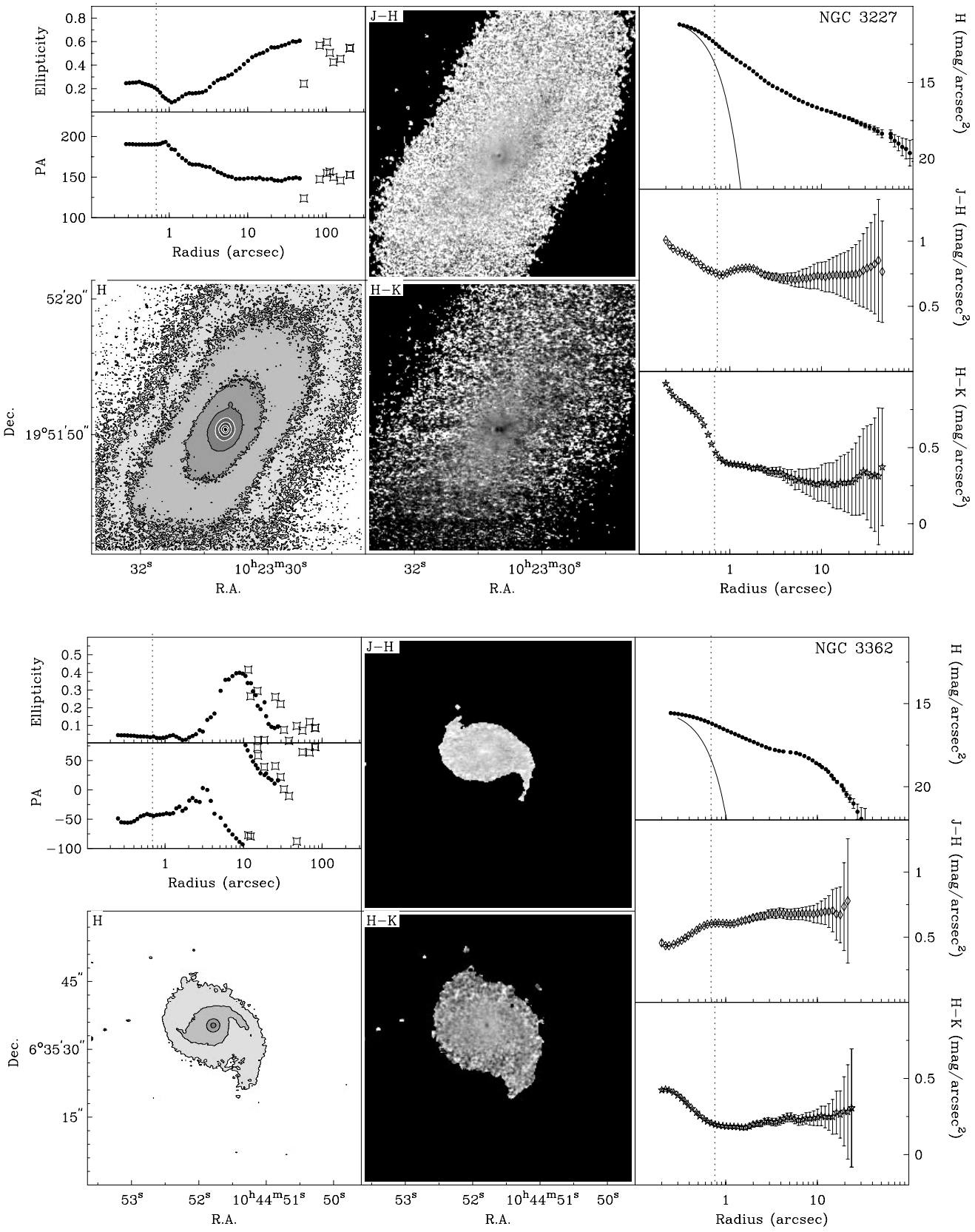

FIG. 1.—*Continued*

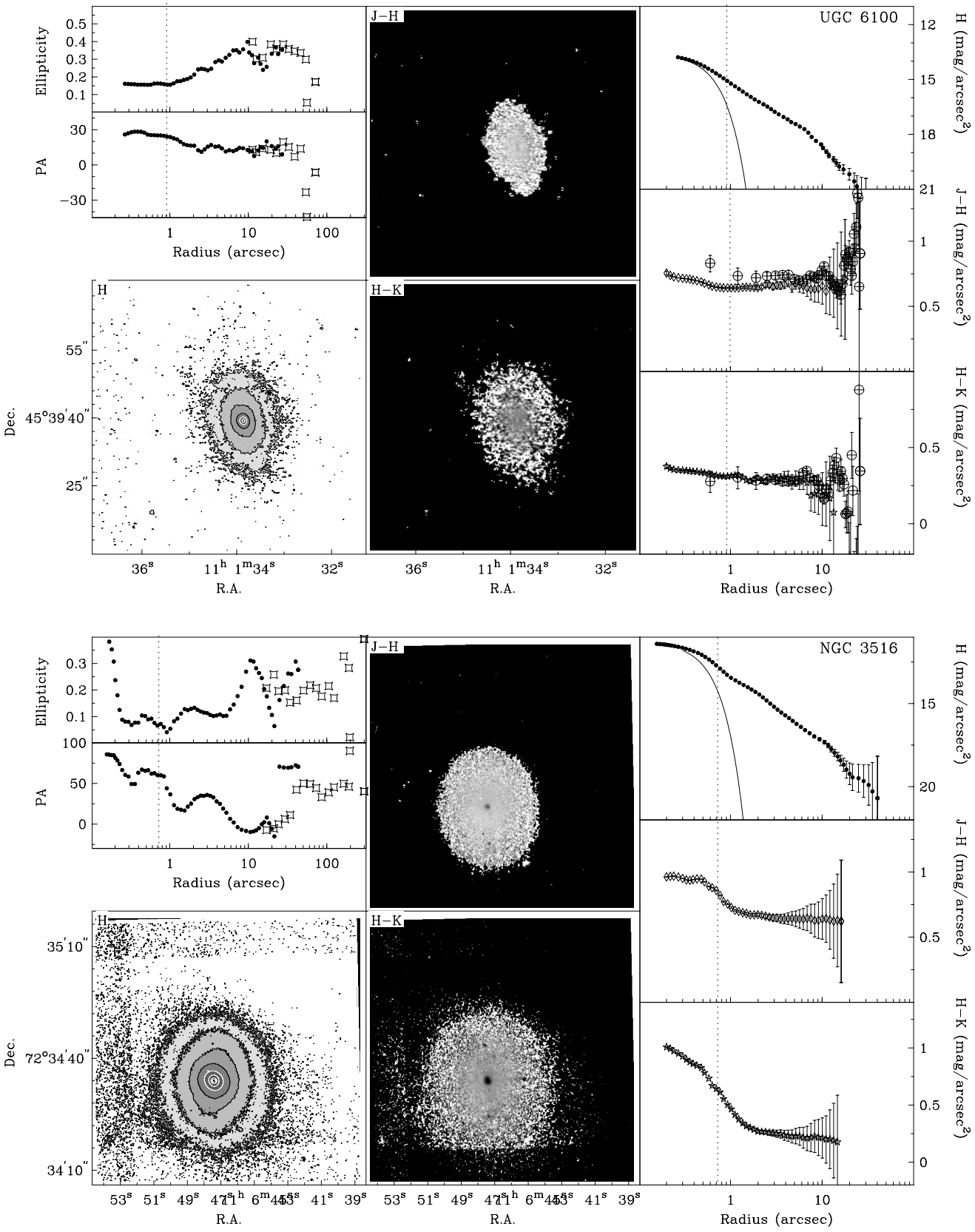

FIG. 1.—*Continued*

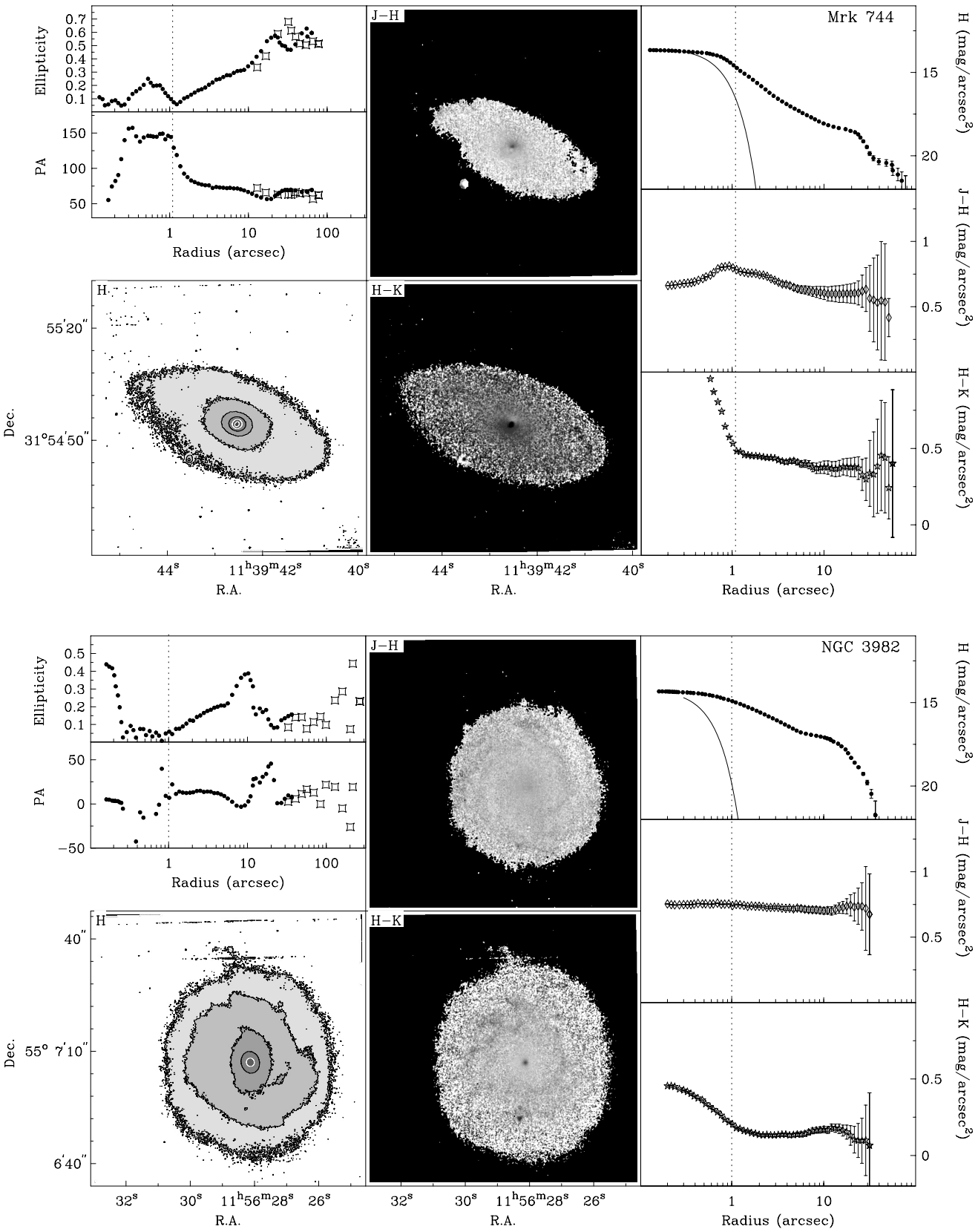

FIG. 1.—*Continued*

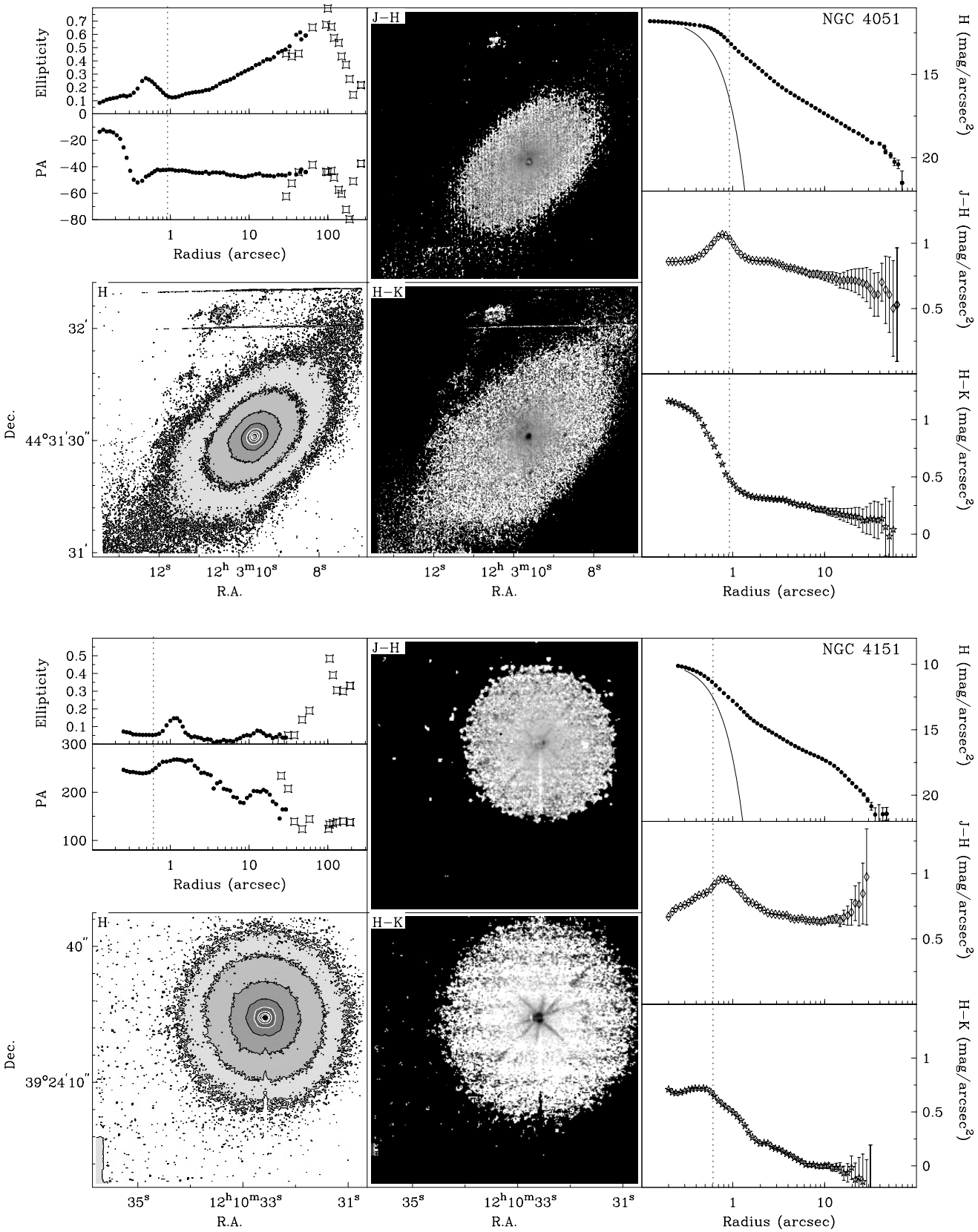

FIG. 1.—*Continued*

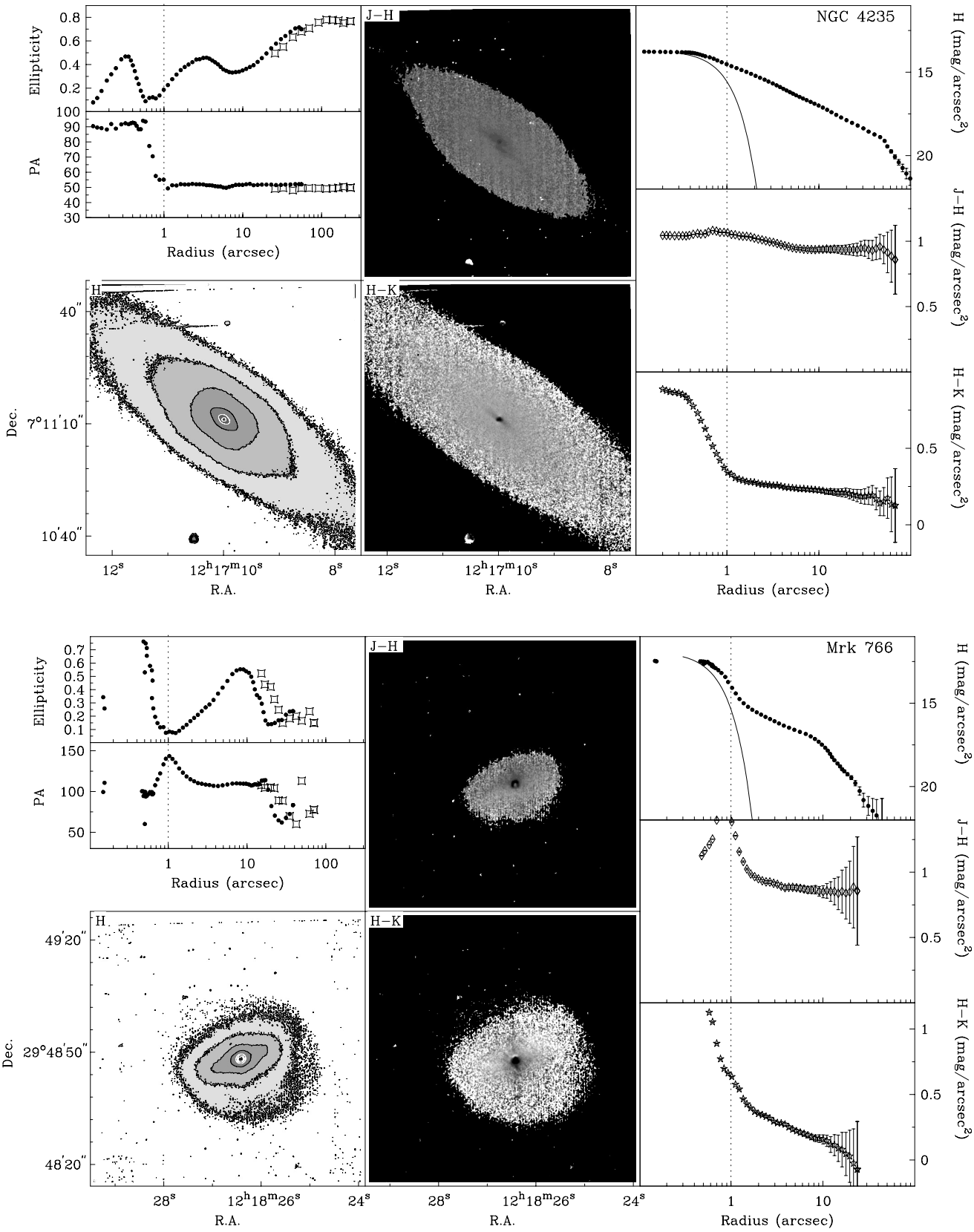

FIG. 1.—*Continued*

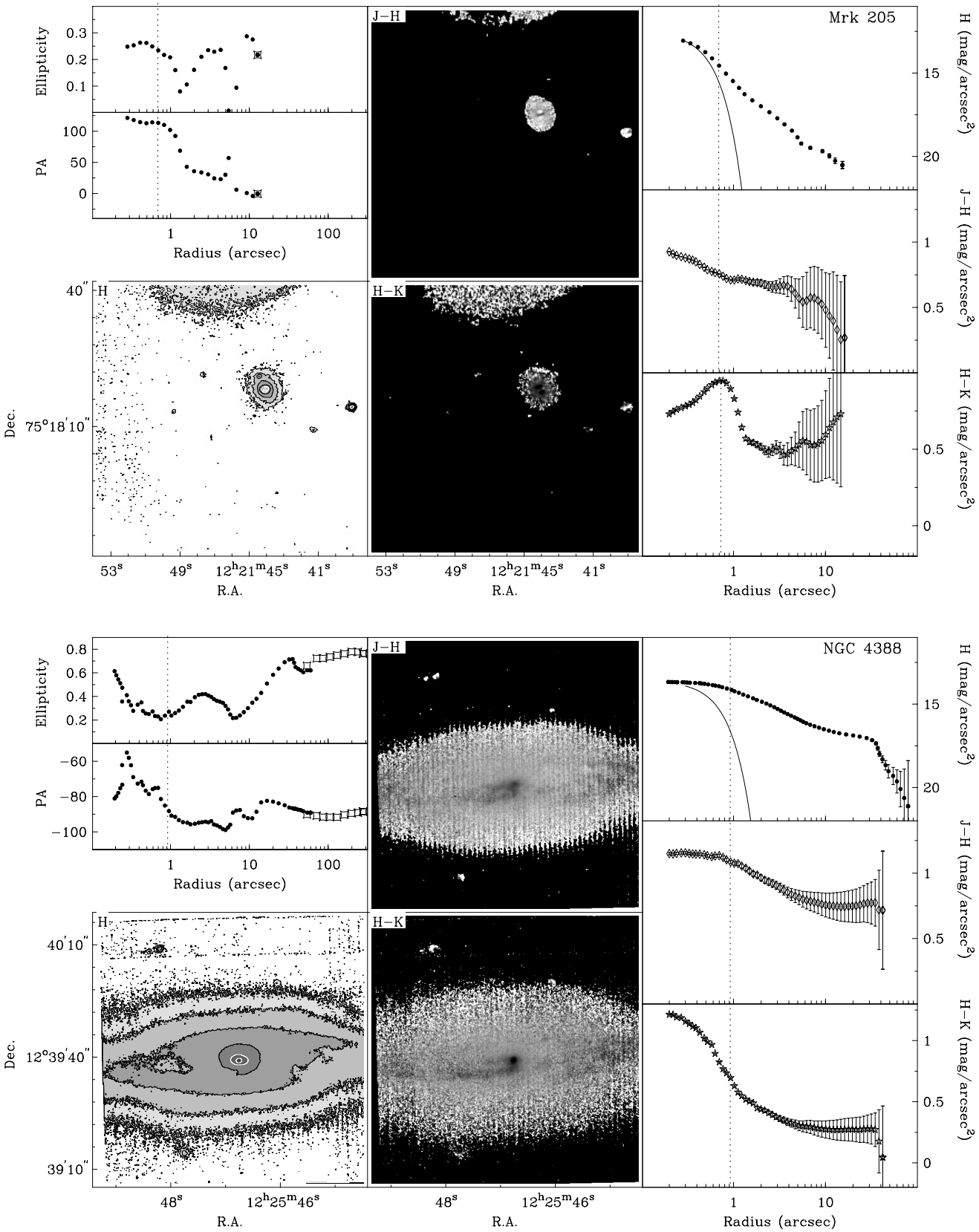

FIG. 1.—*Continued*

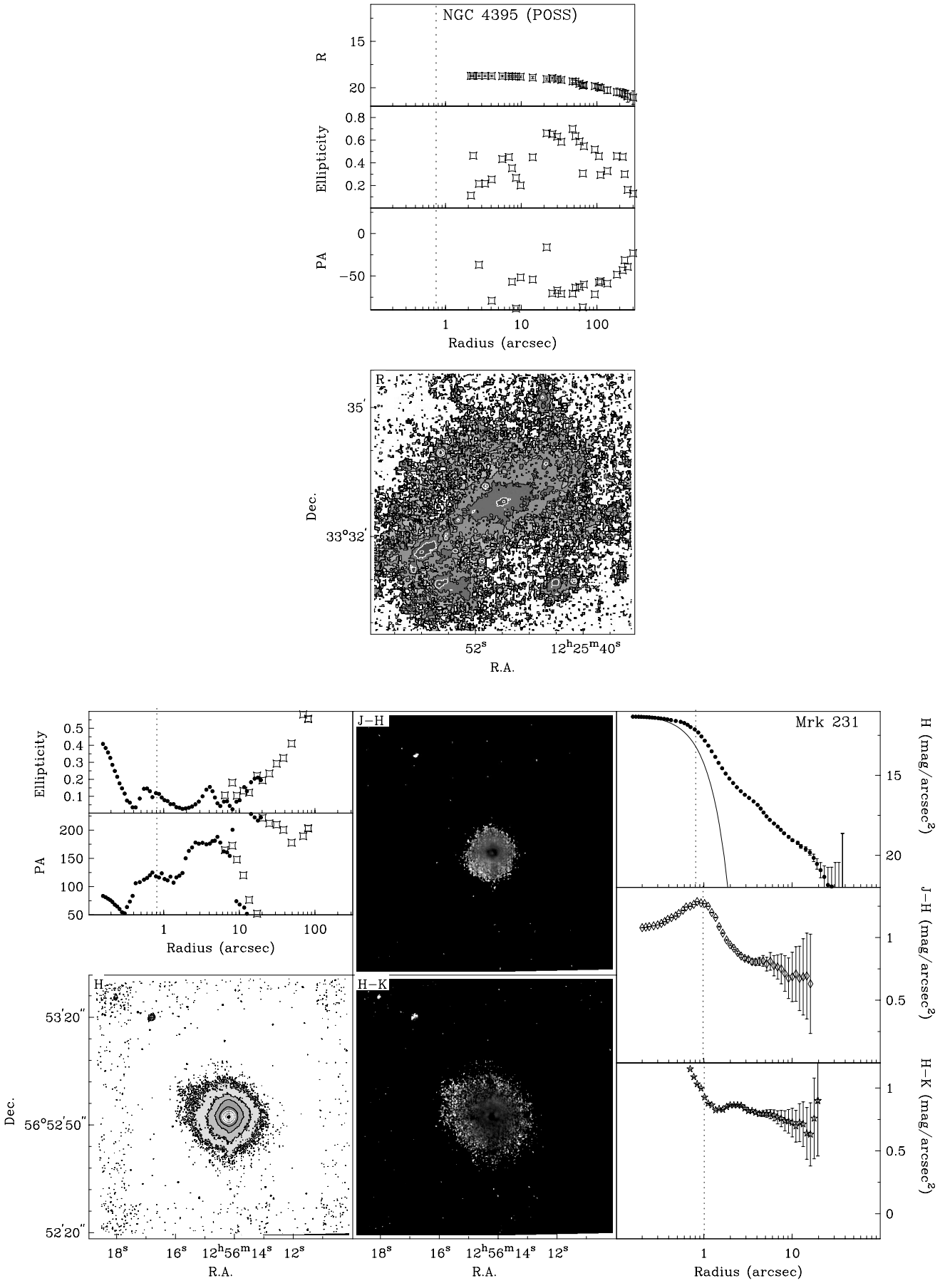

FIG. 1.—*Continued*

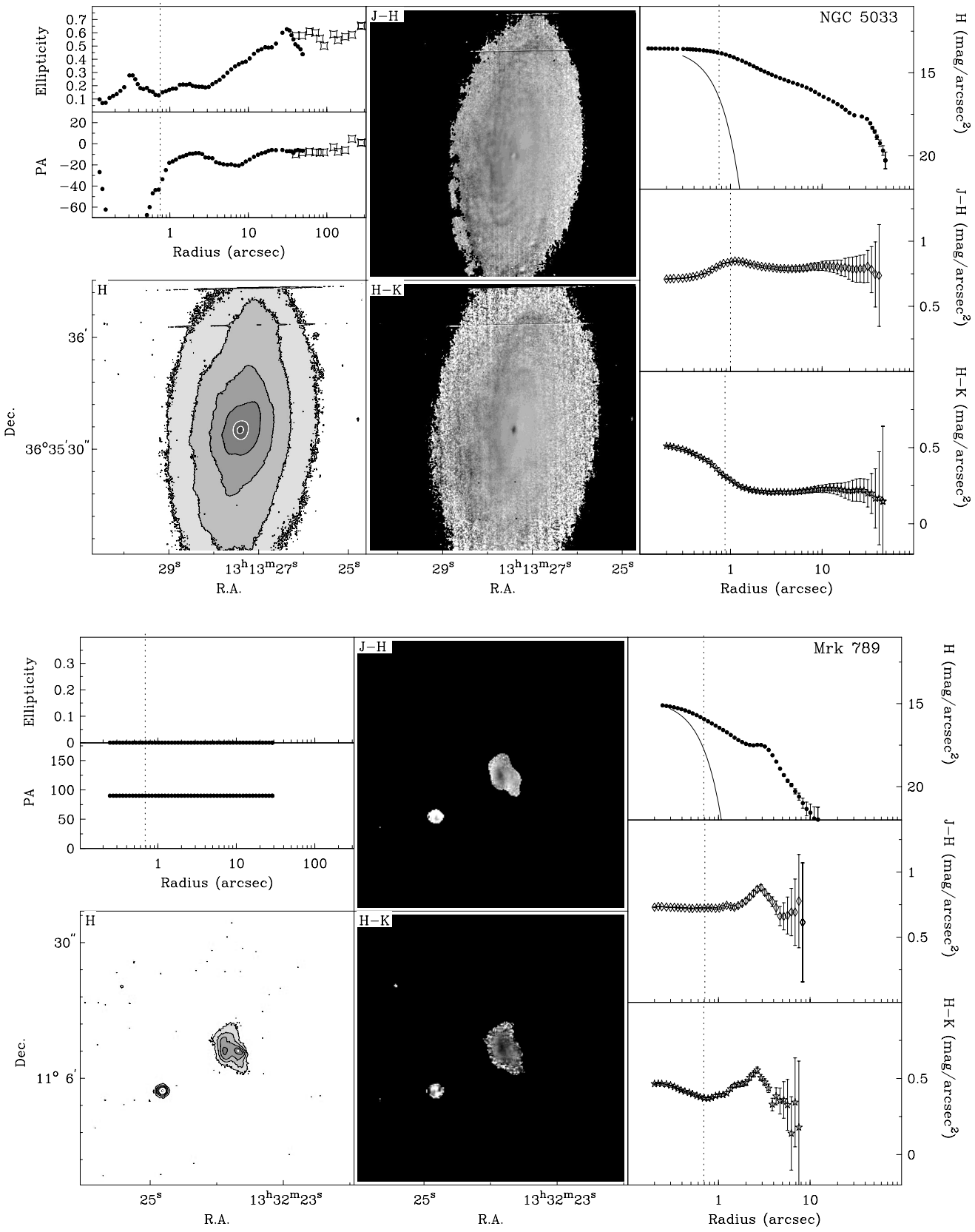

FIG. 1.—*Continued*

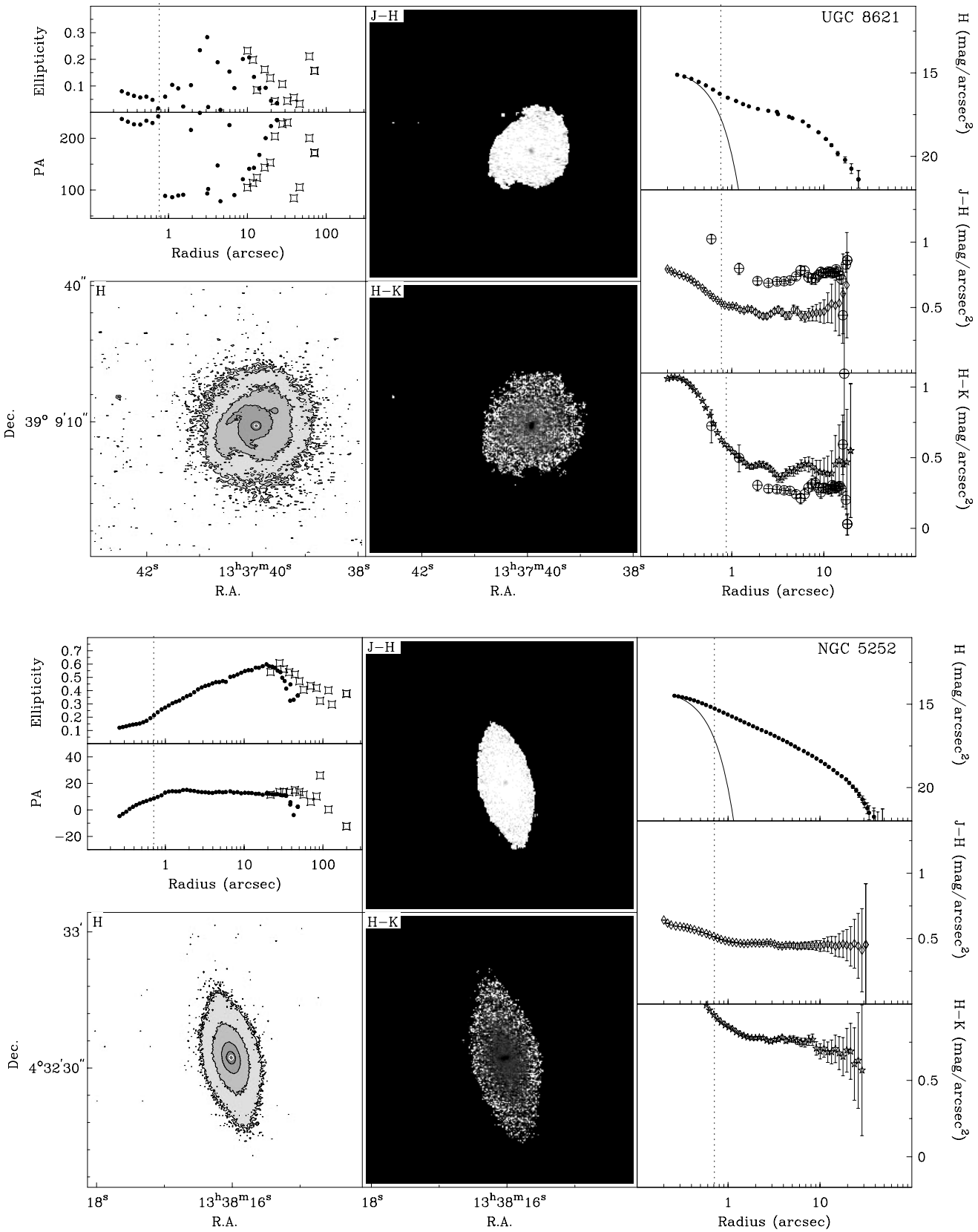

FIG. 1.—*Continued*

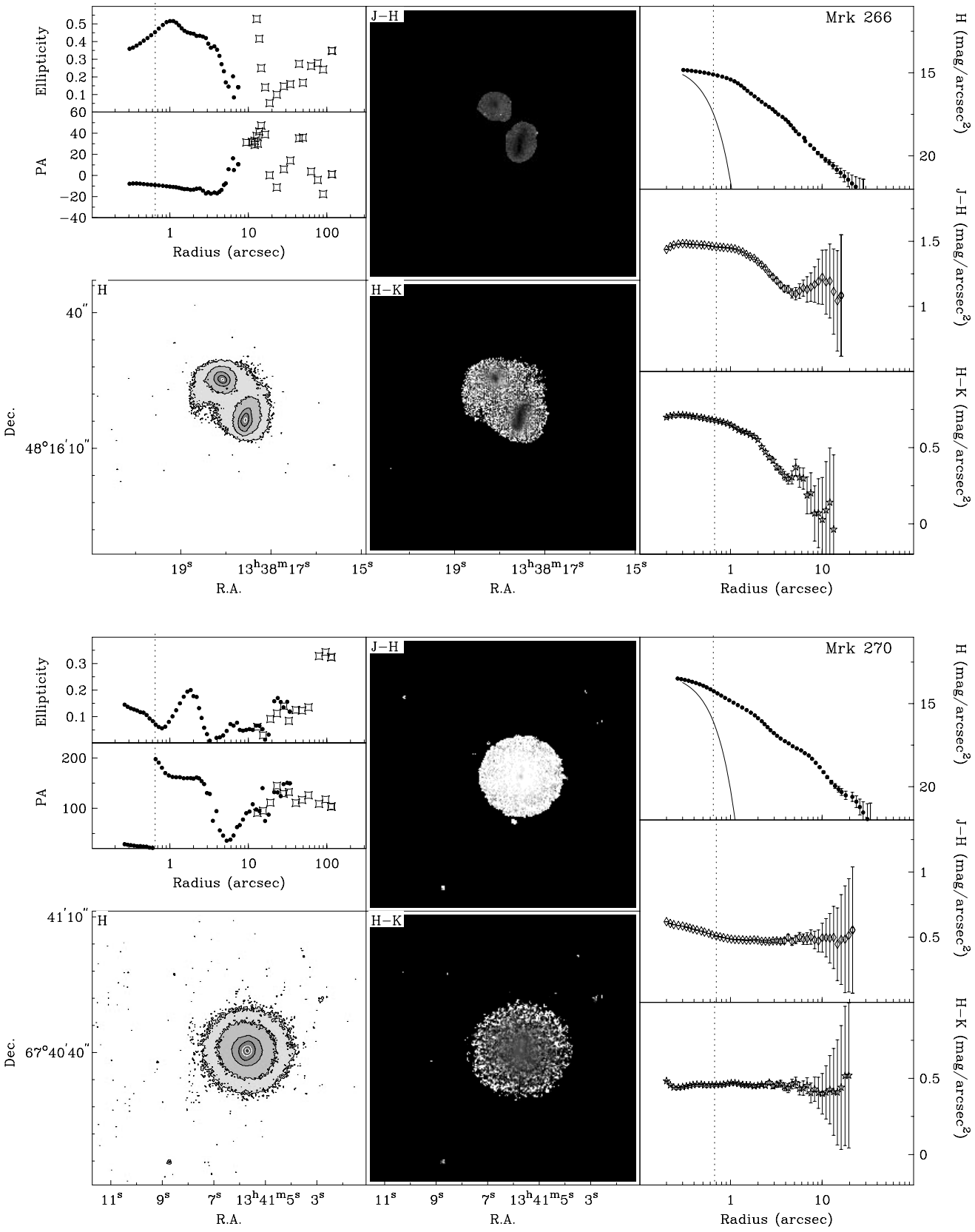

FIG. 1.—*Continued*

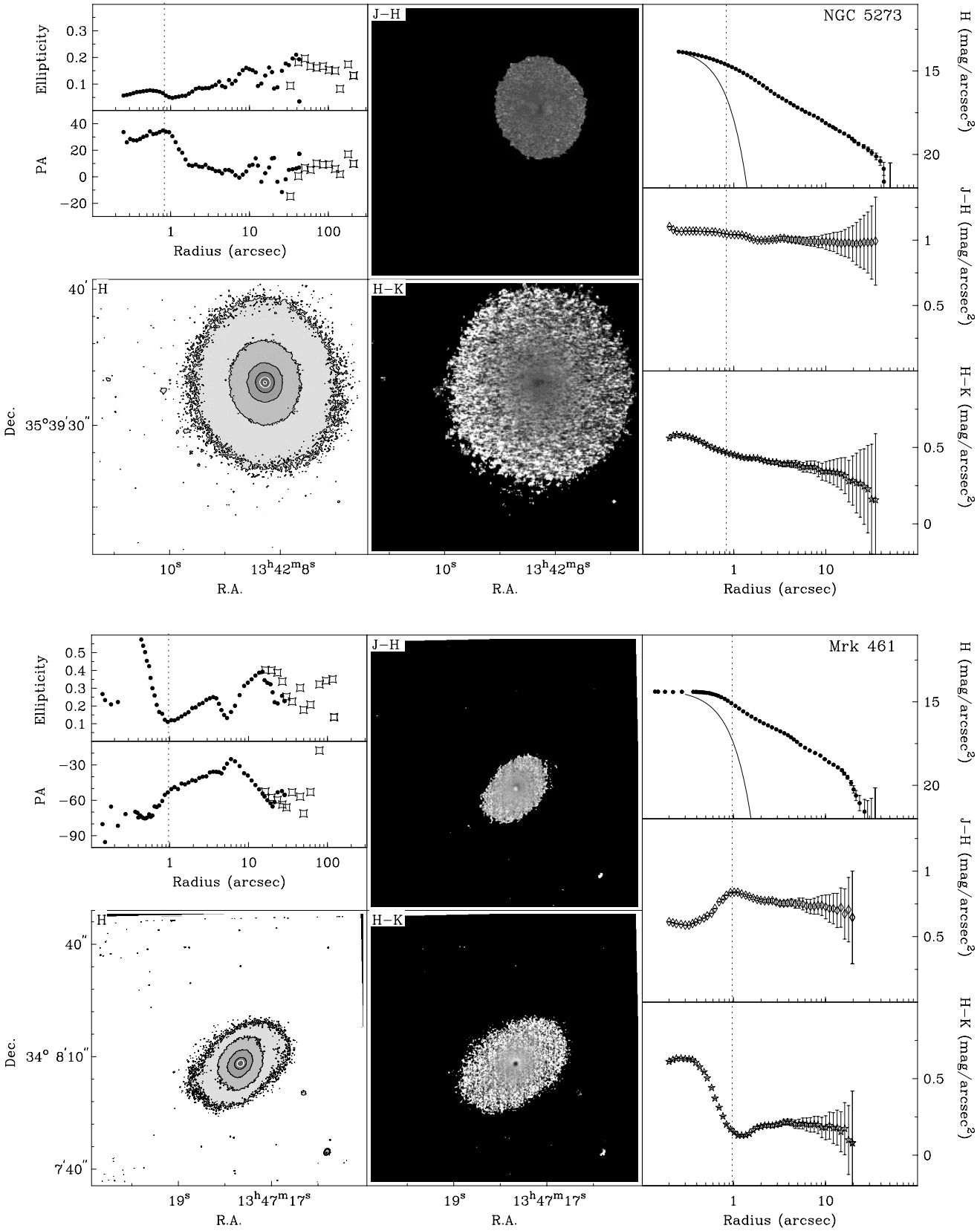

FIG. 1.—*Continued*

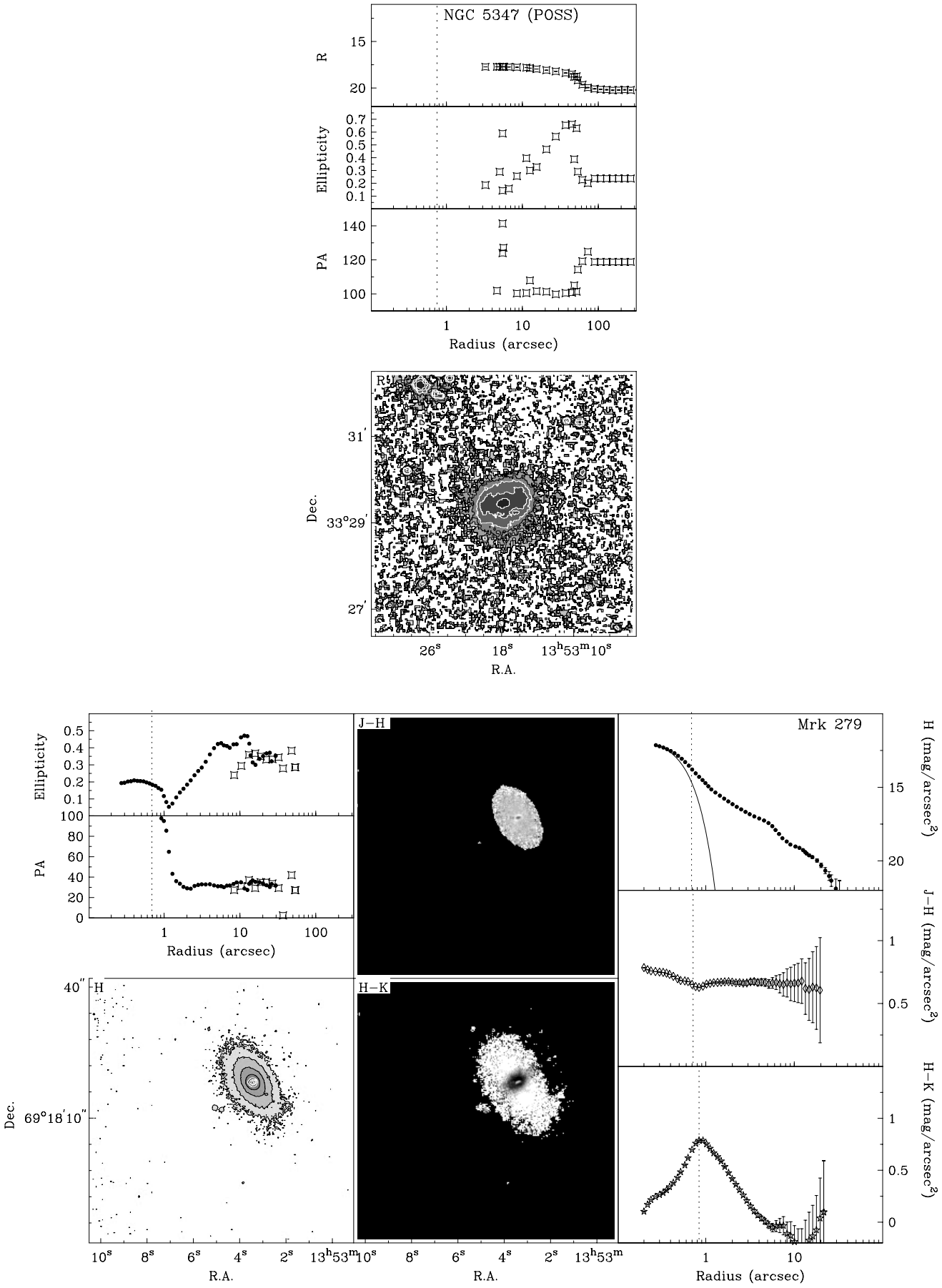

FIG. 1.—*Continued*

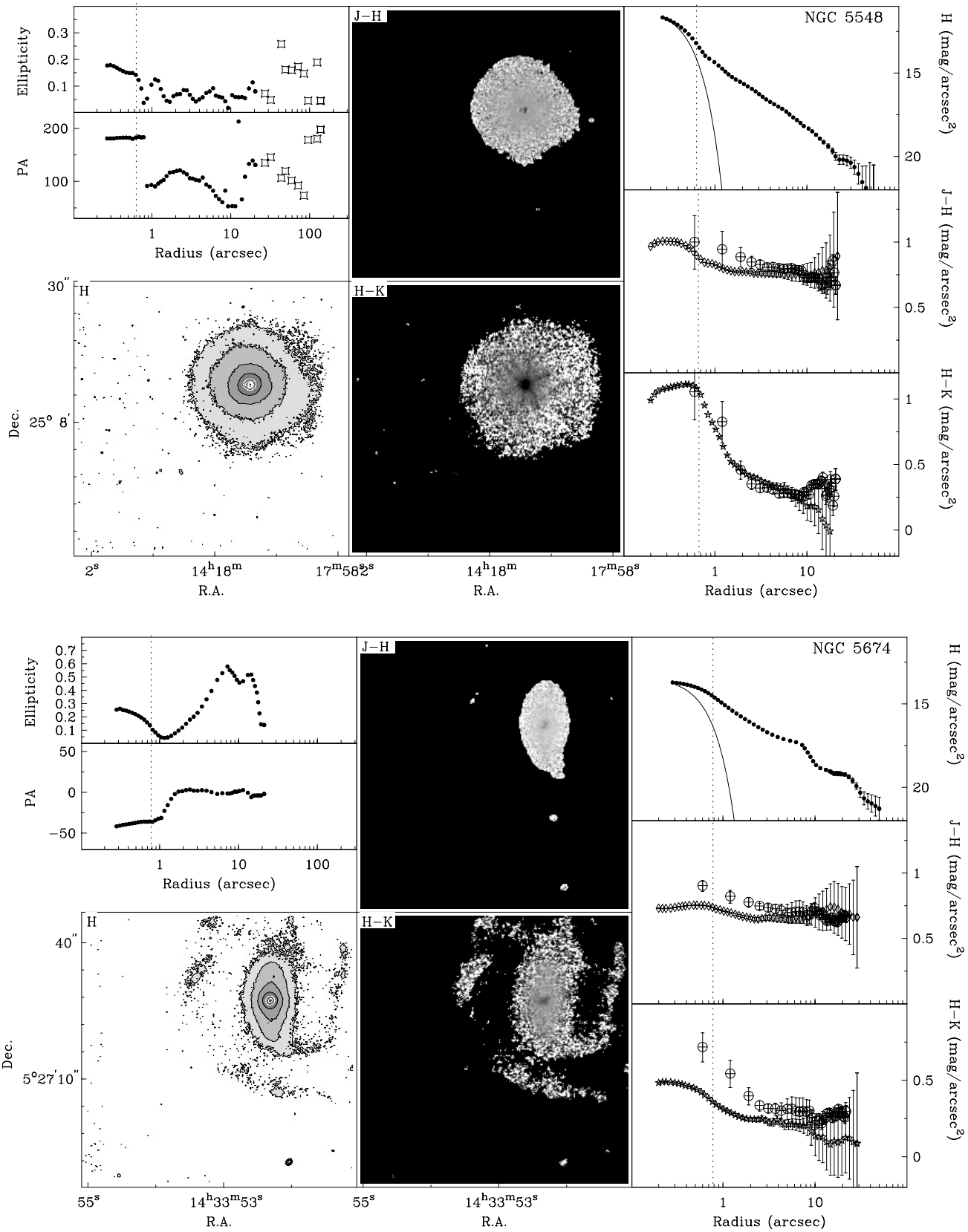

FIG. 1.—*Continued*

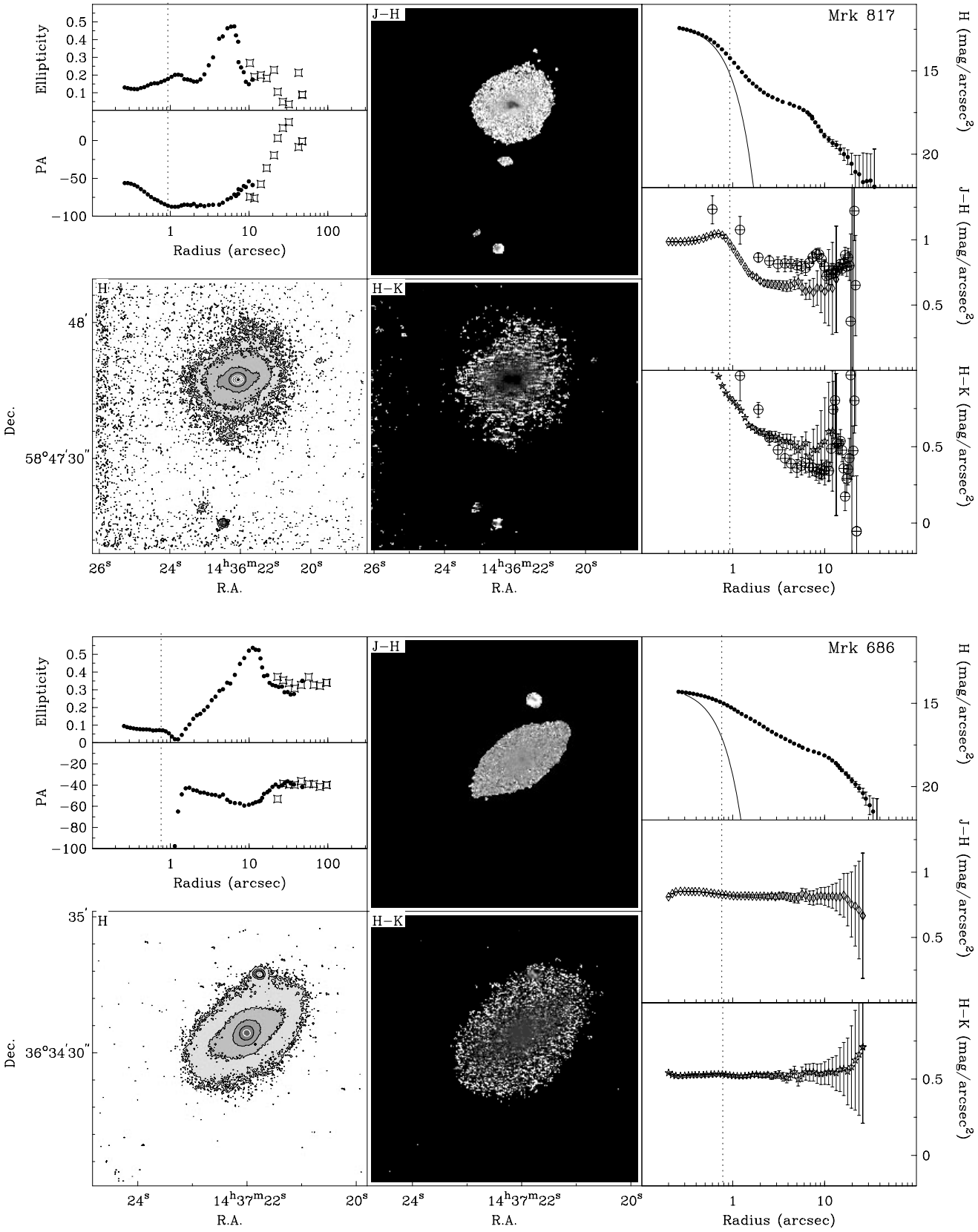

FIG. 1.—*Continued*

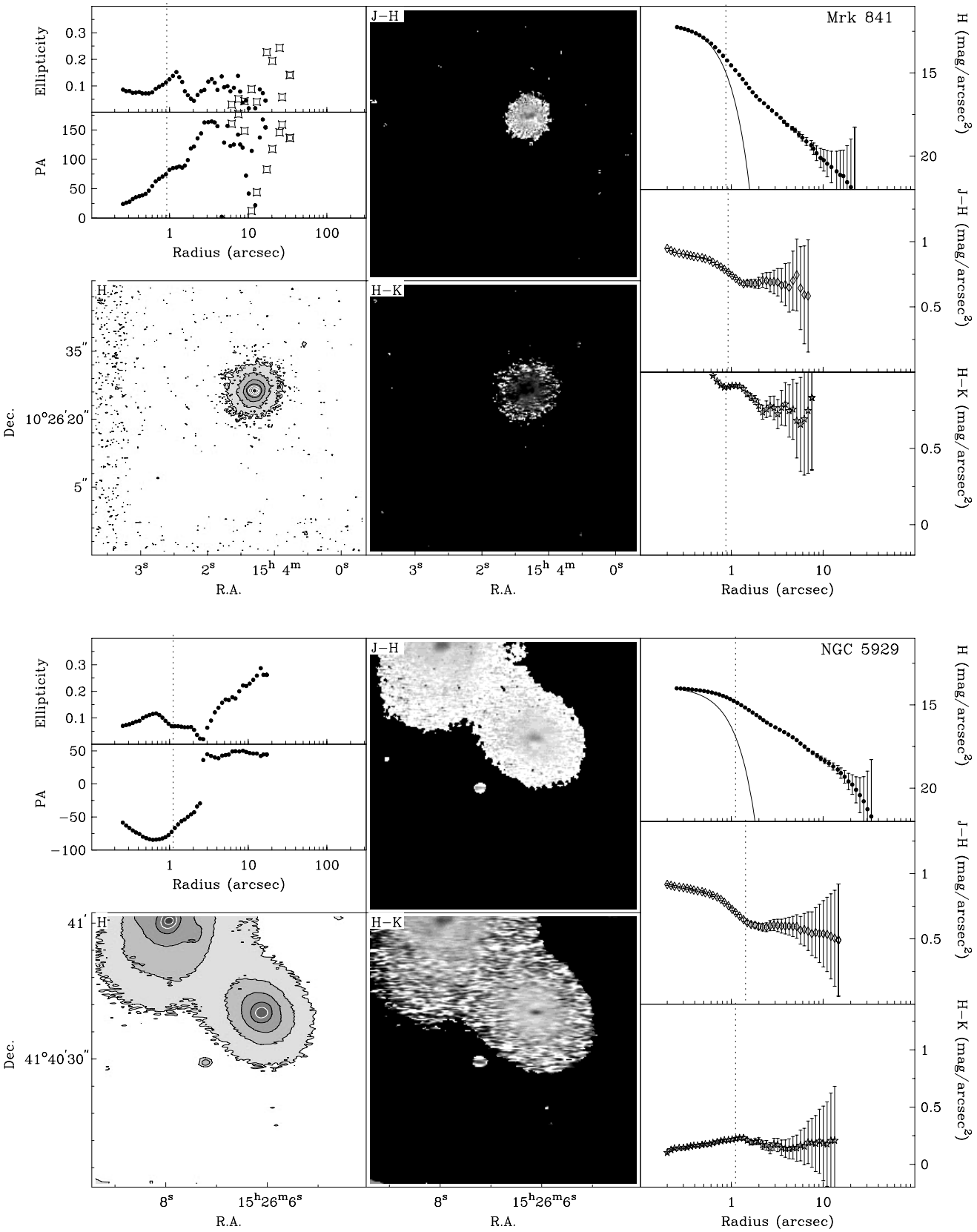

FIG. 1.—*Continued*

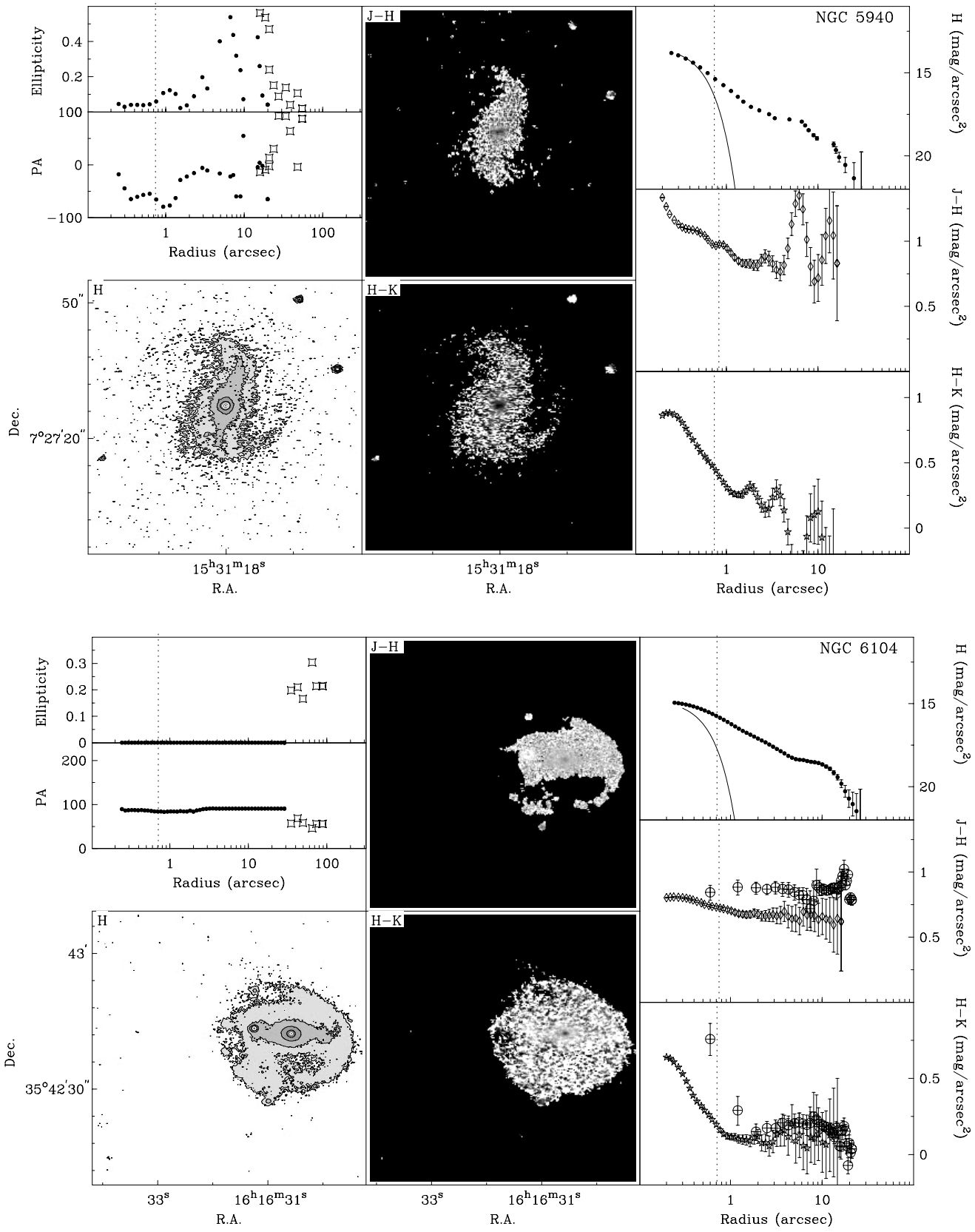

FIG. 1.—*Continued*

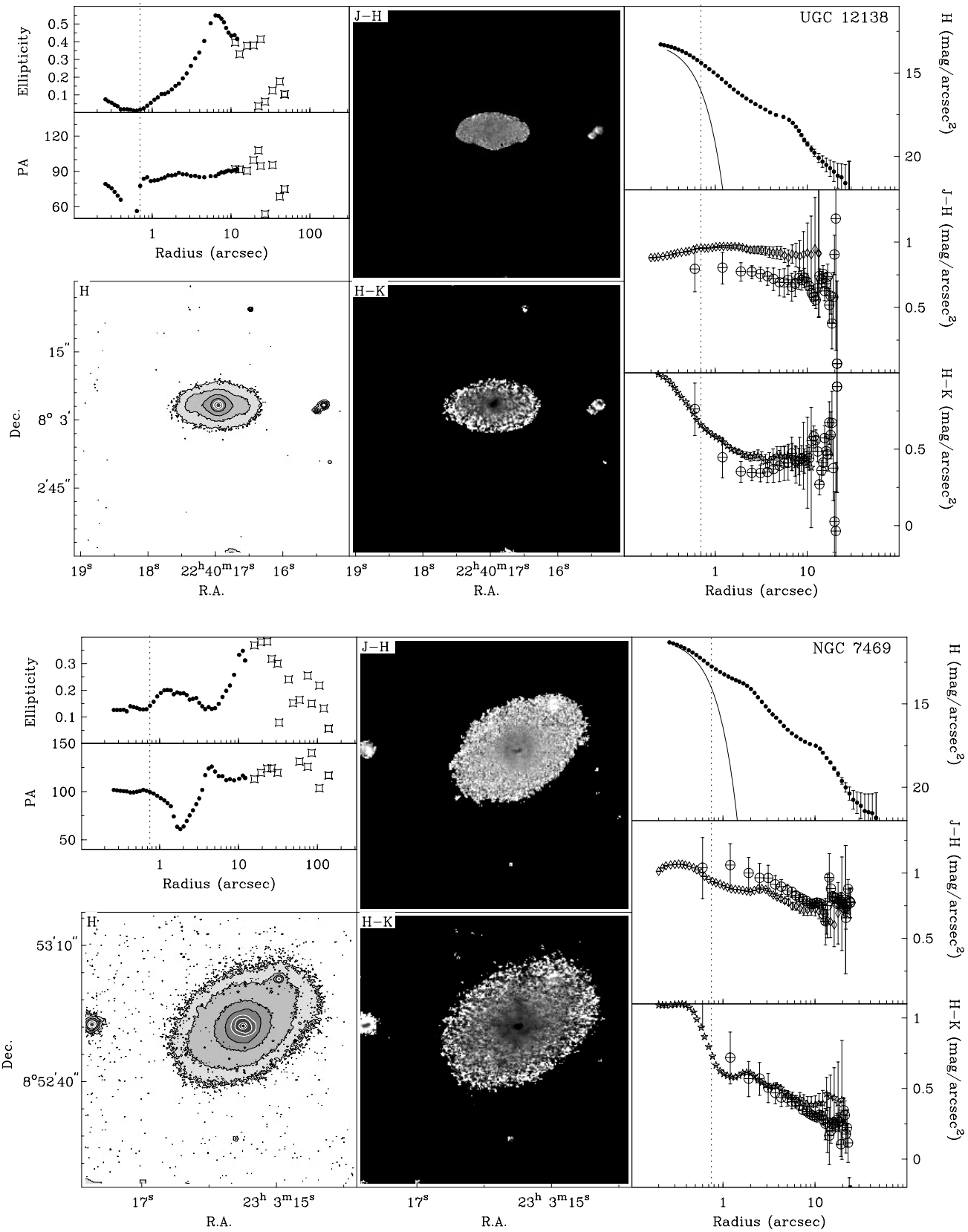

FIG. 1.—*Continued*

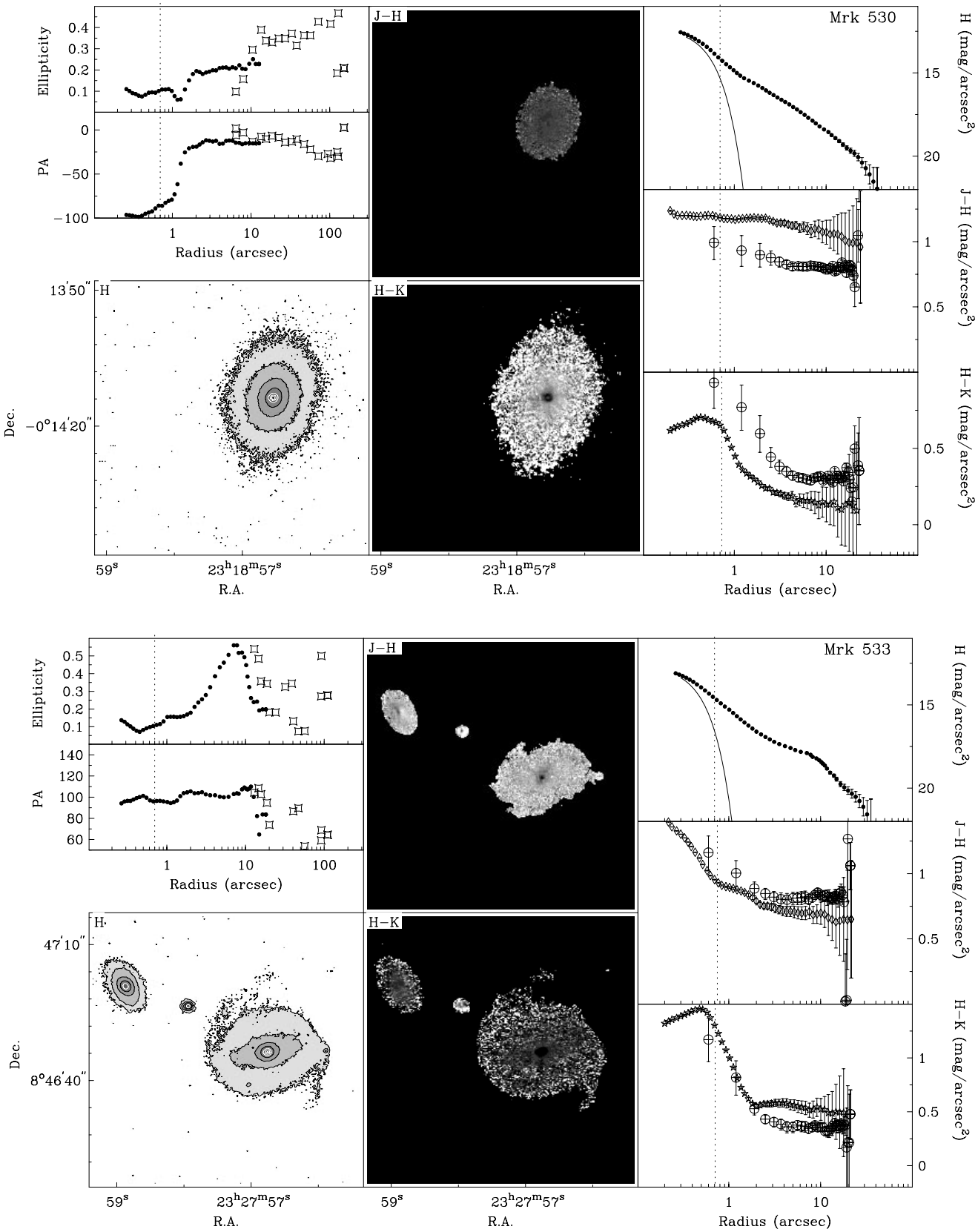

FIG. 1.—*Continued*

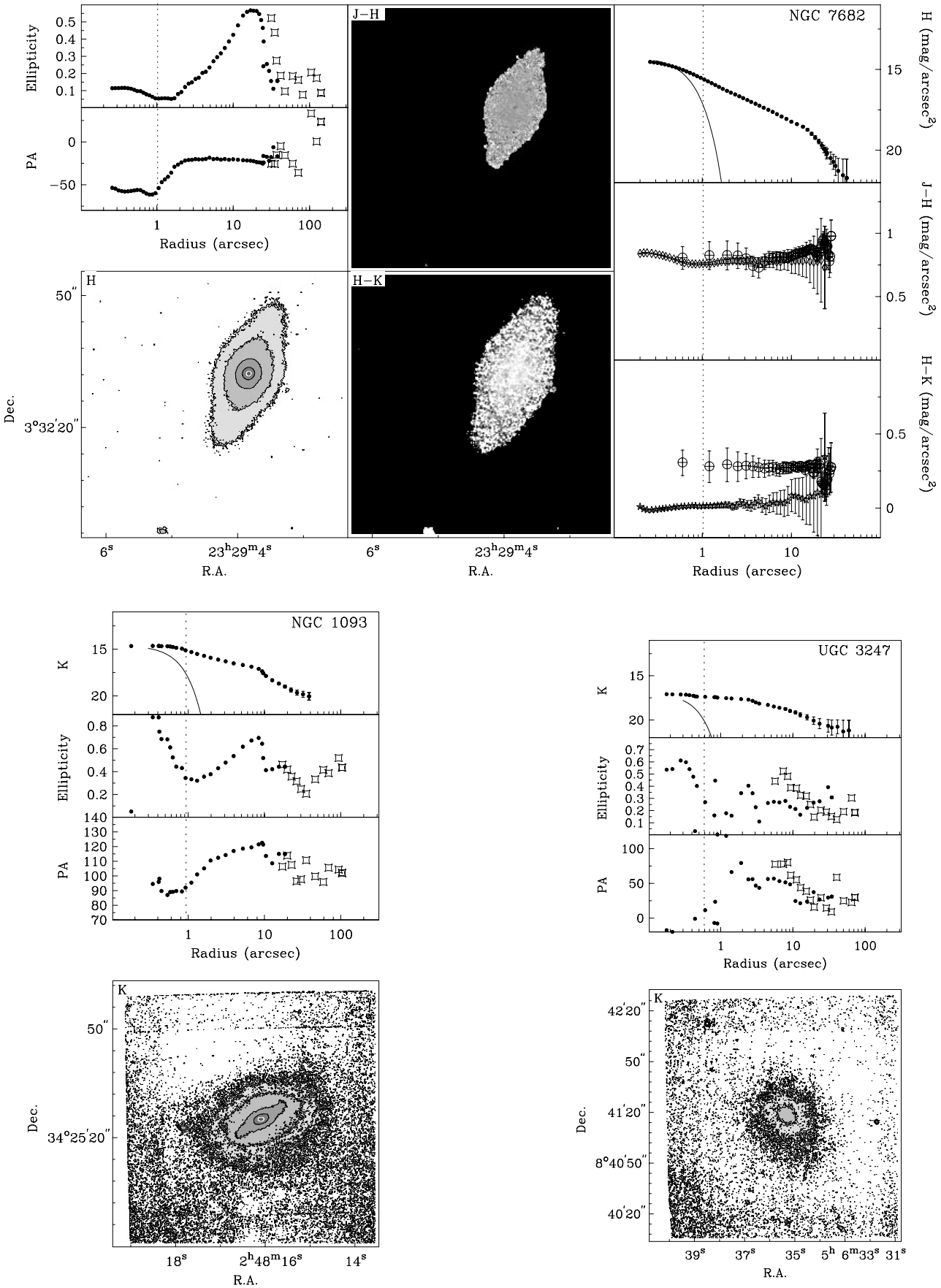

FIG. 1.—*Continued*

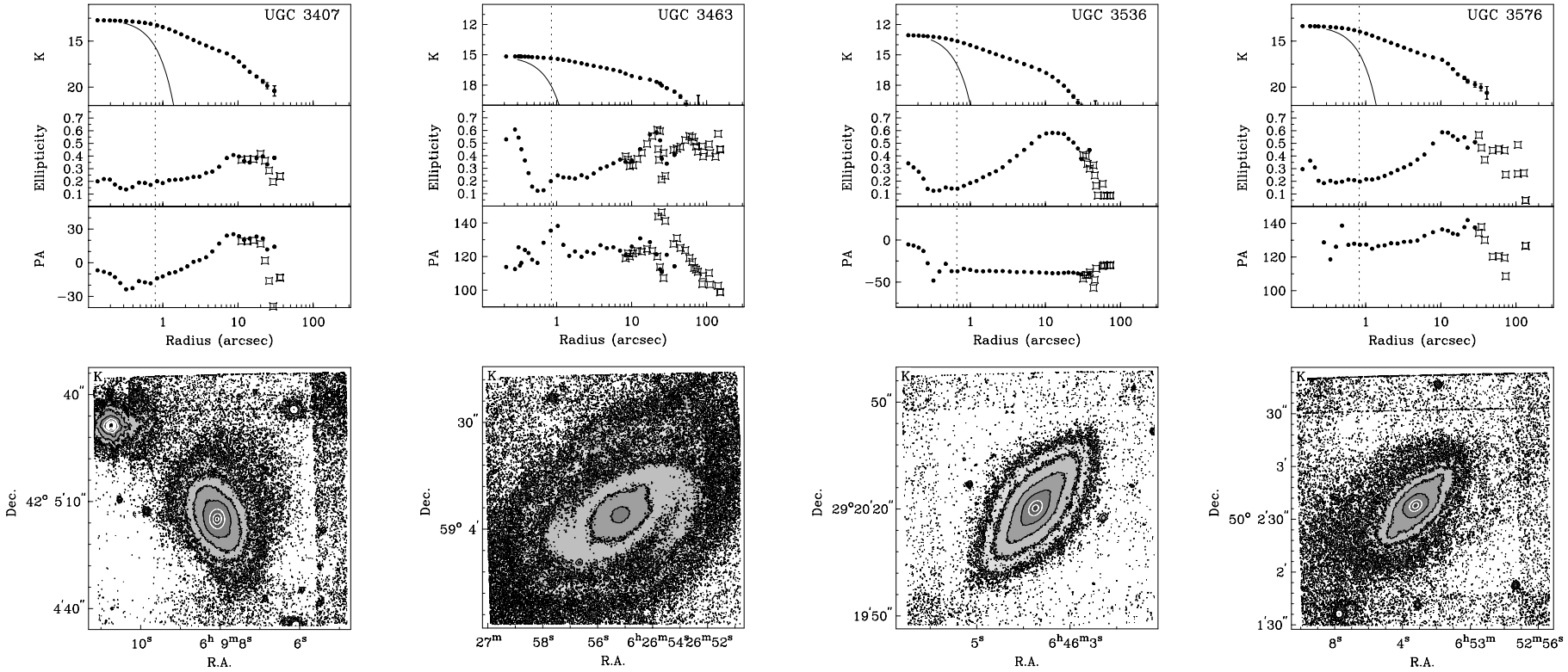

FIG. 1.—*Continued*

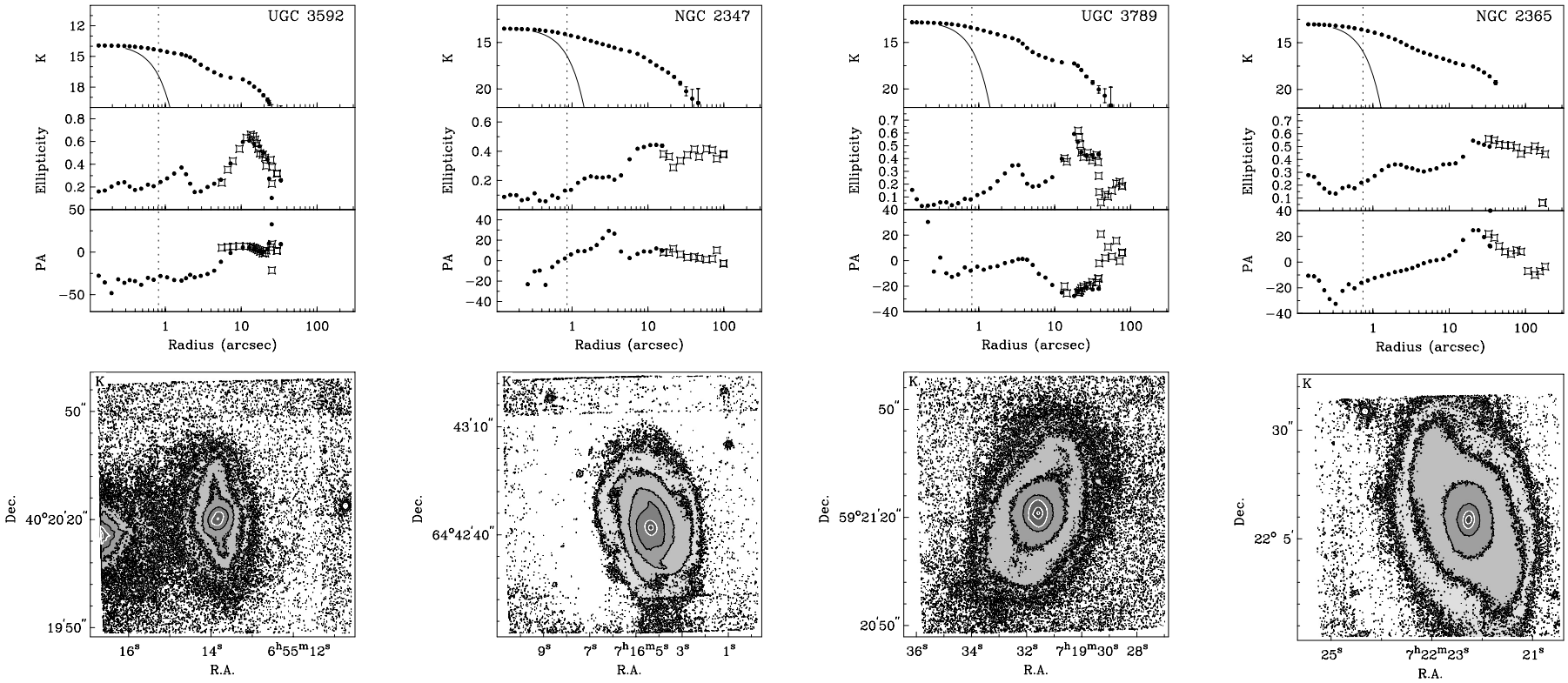

FIG. 1.—*Continued*

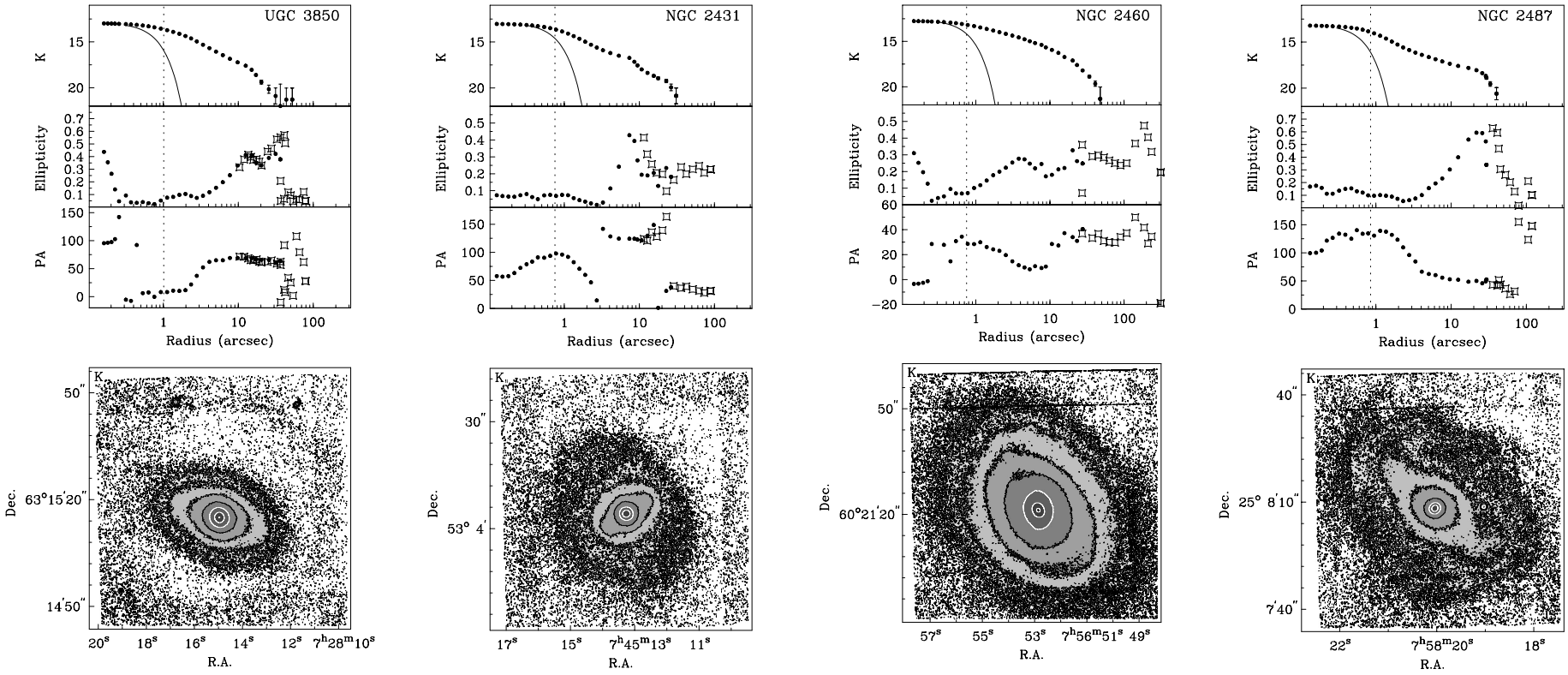

FIG. 1.—*Continued*

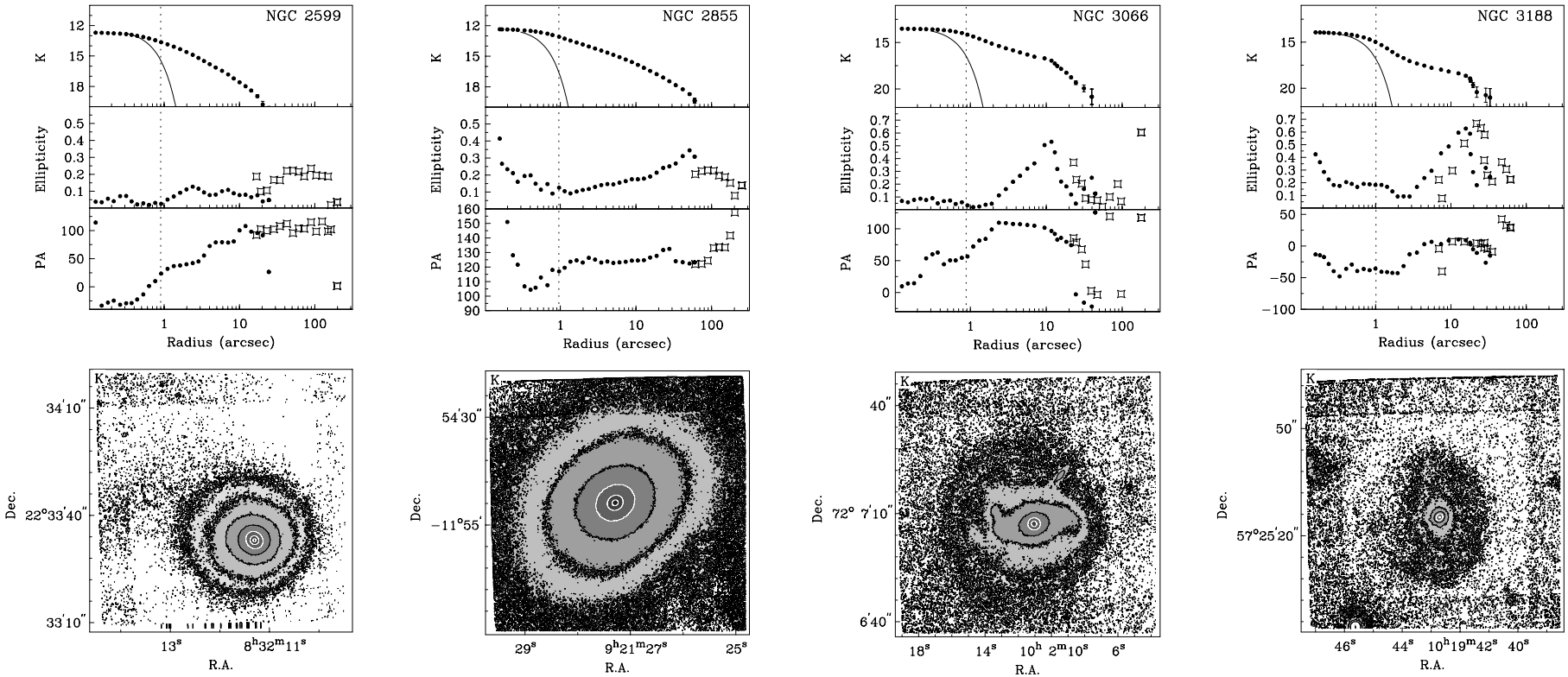

FIG. 1.—*Continued*

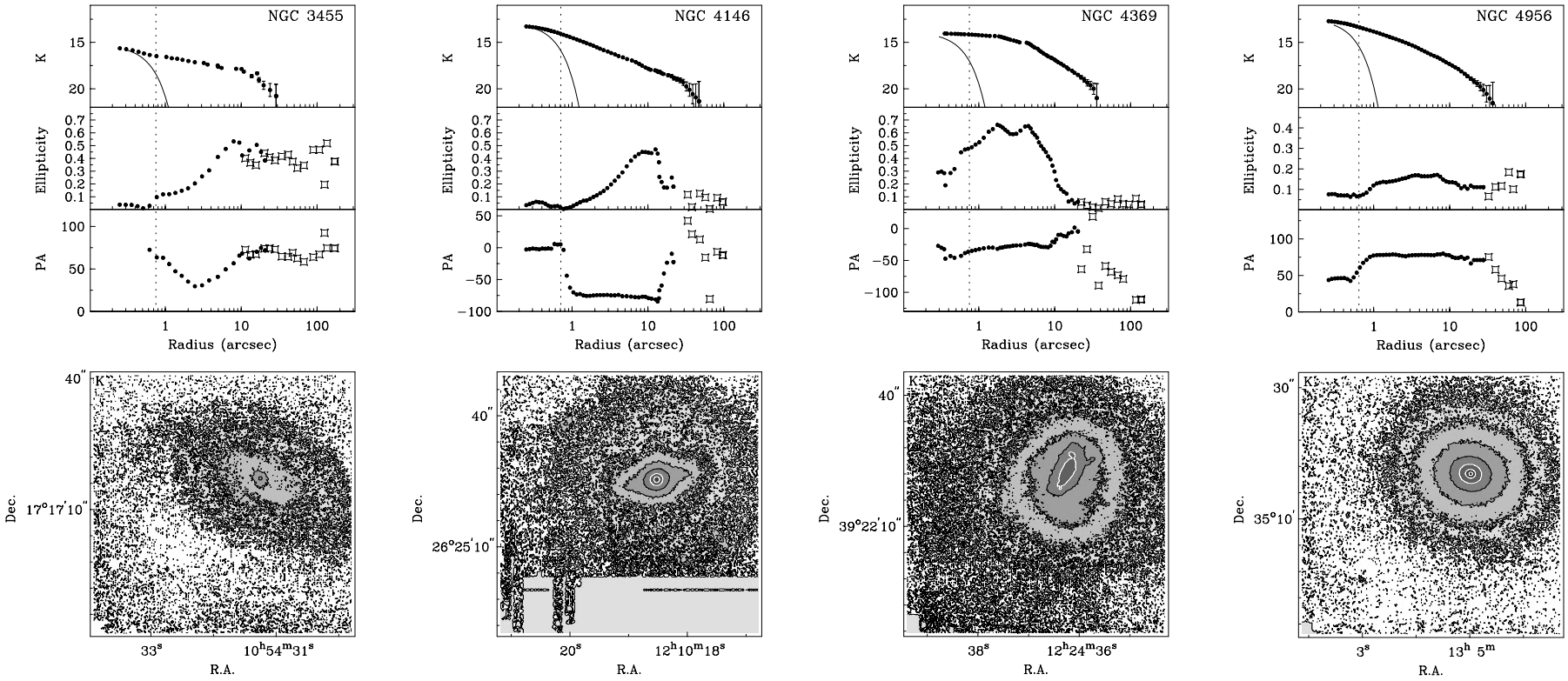

FIG. 1.—*Continued*

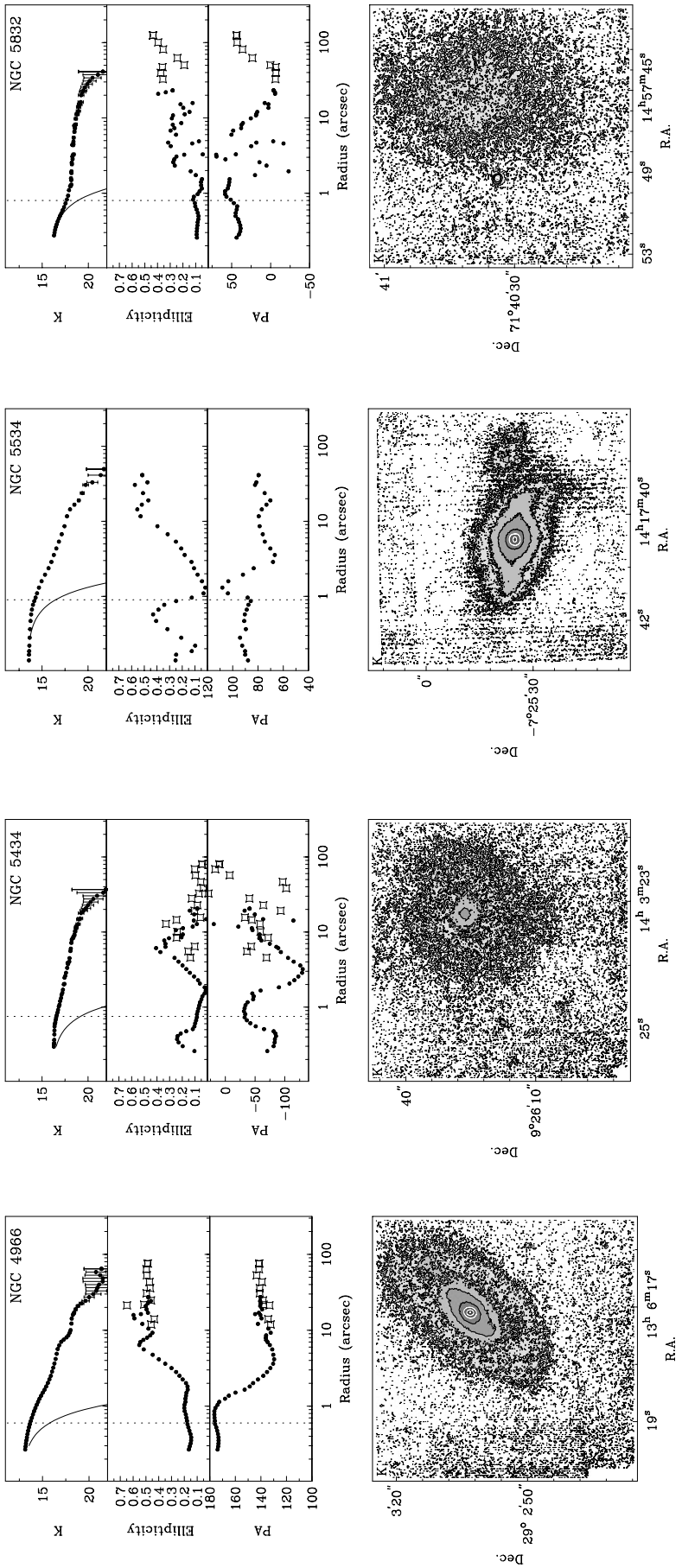

FIG. 1.—*Continued*

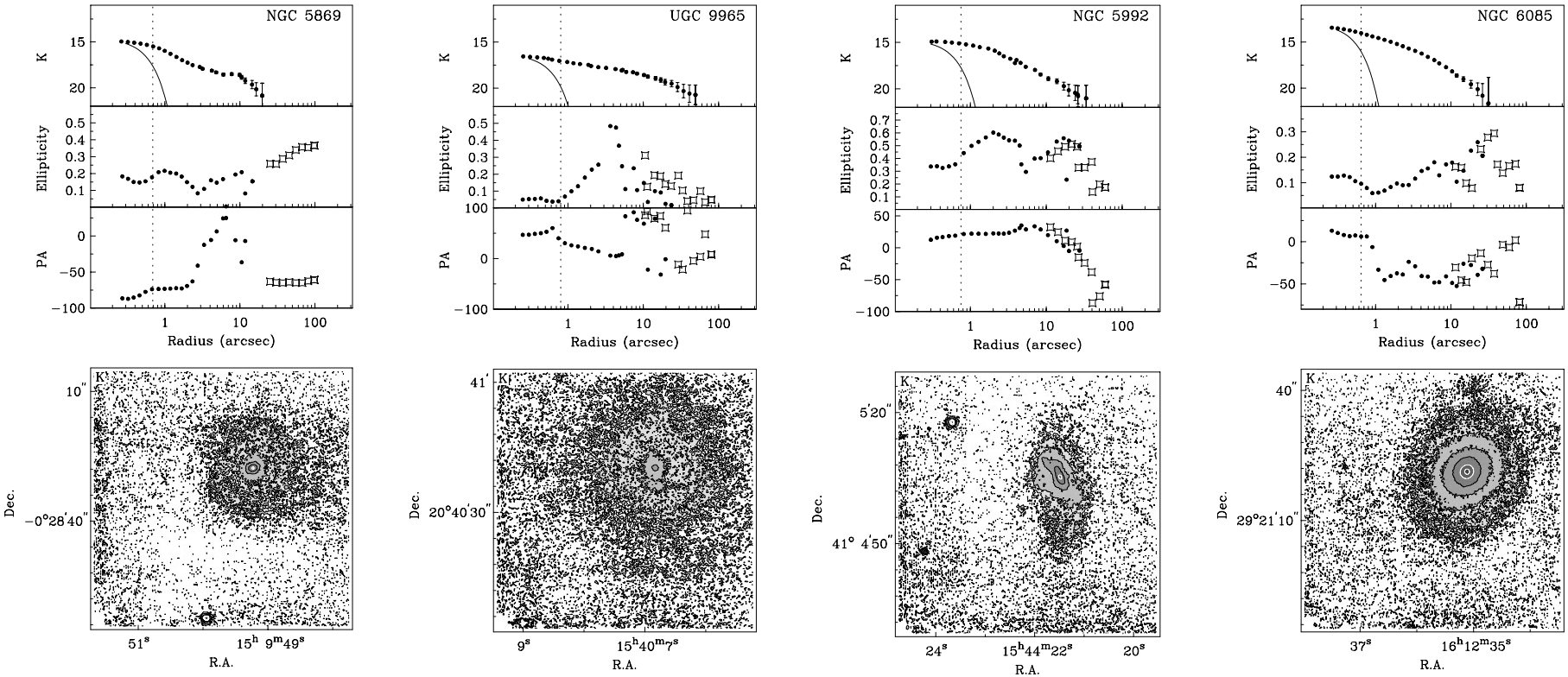

FIG. 1.—*Continued*

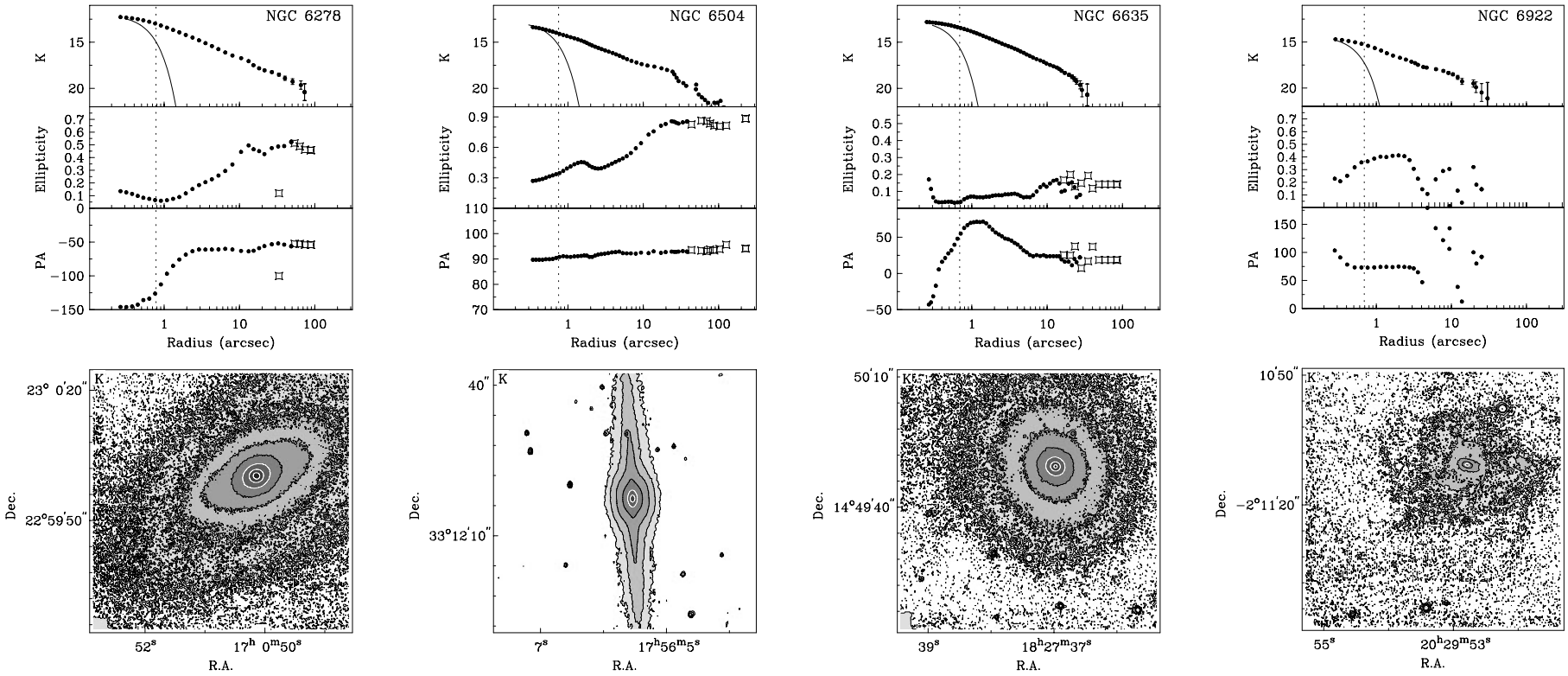

FIG. 1.—*Continued*

TABLE 5

IMAGES AND PHOTOMETRIC PROFILES FOR THE INDIVIDUAL GALAXIES: NGC 1093–NGC 6922

Radius (arcsec)	μ_H	±	$J-H$	±	$H-K$	±	ϵ	ϕ	ϵ(POSS)	ϕ(POSS)
					Mrk 334					
0.26	13.36	0.00	0.81	0.00	1.19	0.00	0.12	213.10	...	...
0.29	13.40	0.00	0.81	0.00	1.20	0.00	0.12	211.70	...	...
0.32	13.44	0.00	0.81	0.00	1.21	0.00	0.13	212.50	...	...
0.35	13.48	0.00	0.82	0.00	1.22	0.00	0.13	211.90	...	...
0.38	13.53	0.00	0.82	0.00	1.22	0.00	0.13	211.50	...	...
0.42	13.59	0.00	0.83	0.00	1.23	0.00	0.12	212.40	...	...
0.46	13.66	0.00	0.84	0.00	1.23	0.00	0.11	213.50	...	...
0.50	13.74	0.00	0.86	0.00	1.23	0.00	0.10	217.30	...	...
0.55	13.83	0.00	0.87	0.00	1.23	0.00	0.07	221.70	...	...
0.60	13.93	0.00	0.89	0.00	1.21	0.00	0.05	227.00	...	...
0.65	14.04	0.00	0.91	0.00	1.19	0.00	0.04	53.20	...	...
0.71	14.17	0.00	0.92	0.00	1.17	0.00	0.03	72.30	...	...
0.78	14.32	0.00	0.94	0.00	1.13	0.00	0.04	89.10	...	...
0.87	14.48	0.00	0.95	0.00	1.07	0.00	0.05	98.90	...	...
0.96	14.65	0.00	0.95	0.00	1.00	0.00	0.06	105.00	...	...
1.06	14.84	0.00	0.96	0.00	0.91	0.00	0.07	107.10	...	...
1.17	15.04	0.00	0.95	0.01	0.81	0.00	0.08	106.80	...	...
1.29	15.26	0.00	0.95	0.01	0.71	0.01	0.09	106.20	...	...
1.43	15.48	0.00	0.93	0.01	0.62	0.01	0.09	103.90	...	...
1.57	15.71	0.00	0.92	0.01	0.53	0.01	0.09	104.80	...	...
1.74	15.93	0.01	0.89	0.01	0.45	0.01	0.10	106.80	...	...
1.92	16.15	0.01	0.87	0.02	0.38	0.02	0.11	108.50	...	...
2.14	16.35	0.01	0.85	0.02	0.33	0.02	0.13	115.40	...	...
2.38	16.54	0.01	0.81	0.02	0.36	0.03	0.15	118.20	...	...
2.64	16.73	0.01	0.79	0.02	0.37	0.03	0.17	119.30	...	...
2.91	16.91	0.01	0.78	0.03	0.38	0.03	0.17	119.60	...	...
3.21	17.10	0.02	0.74	0.03	0.40	0.04	0.17	115.80	...	...
3.47	17.28	0.02	0.71	0.04	0.40	0.05	0.14	103.80	...	...
3.87	17.46	0.03	0.69	0.05	0.41	0.05	0.17	96.90	...	...
4.35	17.64	0.03	0.69	0.05	0.40	0.07	0.20	90.40	...	...
5.03	17.80	0.03	0.68	0.06	0.39	0.08	0.28	86.30	...	...
5.62	17.99	0.04	0.66	0.07	0.36	0.09	0.30	87.10	...	...
6.23	18.19	0.05	0.65	0.09	0.37	0.11	0.31	90.90	...	...
6.85	18.39	0.06	0.64	0.10	0.39	0.13	0.31	92.20	...	...
7.68	18.53	0.07	0.62	0.12	0.34	0.16	0.34	96.50	...	...
8.42	18.70	0.08	0.61	0.13	0.35	0.18	0.33	104.30	...	...
9.00	18.89	0.09	0.61	0.16	0.35	0.21	0.29	108.20	...	...
9.73	19.11	0.11	0.59	0.20	0.35	0.27	0.27	110.50	0.43	89.70
10.44.....	19.38	0.14	0.58	0.24	0.37	0.32	0.23	113.80	0.45	93.42
11.74.....	19.61	0.18	0.58	0.30	0.41	0.40	0.26	110.60	0.39	101.61
12.91.....	19.87	0.23	0.55	0.37	0.43	0.49	...	...	0.31	107.21
14.20.....	20.13	0.29	0.53	0.46	0.49	0.59	...	...	0.26	110.11
15.62.....	20.43	0.38	0.50	0.59	0.64	0.69	...	...	0.26	118.93
17.18.....	20.74	0.51	0.39	0.73	0.66	0.91	...	...	0.28	130.35
18.90.....	20.91	0.59	0.33	0.79	...	...	...	...	0.26	134.04
20.79.....	20.90	0.59	0.31	0.81	...	...	...	...	0.23	135.29
22.87.....	21.10	0.70	0.29	0.95	...	...	...	...	0.22	149.14
25.16.....	21.38	0.92	...	...	...	...	...	...	0.18	156.57
27.68.....	...	...	...	...	...	...	...	...	−0.51	82.83
30.44.....	...	...	...	...	...	...	...	...	−0.68	42.36
79.14.....	...	...	...	...	...	...	...	...	0.32	172.70

NOTE.—Data plotted in Fig. 1. Only tabulated are data points for which the error in the H-band surface brightness is less than 1 mag. Table 5 is published in its entirety in the electronic edition of The Astrophysical Journal. A portion is shown here for guidance regarding its form and content.

shows that the photometric accuracy of the control sample is about 0.3–0.5 mag. The importance of this number is marginal, however, since no color information is provided for the control sample.

After the photometric calibration, color index maps and profiles were made of the Seyferts. To create color maps, frames in two bands were first sky-subtracted, after which the frame with the best seeing was convolved with a Gaussian to match the circular Gaussian seeing FWHM of both galaxies. The frames were then shifted to the same center, divided by each other, and calibrated.

The resulting color maps are shown in Figure 1. In a few cases some effects of different PSFs are seen in the center, since in general the PSF on the WHT is slightly elliptical

TABLE 6

IMAGES AND PHOTOMETRIC PROFILES FOR THE INDIVIDUAL GALAXIES: NGC 1093–NGC 6922

Radius	μ_H	±	ϵ	ϕ	ϵ (POSS)	ϕ (POSS)
			NGC 1093			
0.34	14.64	0.00	0.88	94.50	...	...
0.41	14.65	0.00	0.88	95.90	...	...
0.18	14.66	0.00	...	...	...	...
0.42	14.66	0.00	0.75	98.10	...	...
0.45	14.67	0.00	0.69	89.70	...	...
0.53	14.68	0.00	0.68	87.00	...	...
0.58	14.71	0.00	0.61	89.00	...	...
0.63	14.77	0.00	0.52	89.10	...	...
0.70	14.85	0.00	0.44	89.70	...	...
0.83	14.94	0.00	0.43	89.40	...	...
0.92	15.12	0.00	0.34	92.00	...	...
1.10	15.30	0.00	0.33	95.40	...	...
1.31	15.51	0.01	0.32	101.00	...	...
1.61	15.71	0.01	0.36	105.10	...	...
1.97	15.91	0.01	0.38	110.50	...	...
2.47	16.12	0.01	0.43	112.40	...	...
3.10	16.30	0.01	0.48	114.20	...	...
3.94	16.51	0.01	0.54	117.00	...	...
5.21	16.69	0.02	0.62	118.60	...	...
6.75	16.88	0.02	0.67	119.50	...	...
8.40	17.10	0.03	0.69	121.50	...	...
9.33	17.37	0.03	0.64	122.60	...	...
9.63	17.57	0.04	0.52	121.40	...	...
10.47	17.86	0.05	0.41	113.60	...	...
12.64	18.33	0.08	0.42	108.60	...	...
15.47	18.68	0.11	0.44	115.00	...	...
18.56	19.00	0.15	0.44	115.00	0.45	112.69
22.27	19.37	0.22	...	...	0.36	108.86
26.73	19.65	0.28	...	...	0.31	96.05
32.07	19.83	0.33	...	...	0.23	102.27
38.49	20.05	0.40	...	...	0.23	110.33
46.18	...	...	...	...	0.33	99.69
55.42	...	...	...	...	0.41	95.07
66.50	...	...	...	...	0.39	102.92
79.80	...	...	...	...	0.42	110.56
93.98	...	...	...	...	0.52	104.30
104.13	...	...	...	...	0.44	102.00

NOTES.—Data plotted in Fig. 1. Only tabulated are data points for which the error in the H-band surface brightness is less than 1 mag. Table 6 is published in its entirety in the electronic edition of The Astrophysical Journal. A portion is shown here for guidance regarding its form and content.

due to telescope movements during the observations, an effect noticed especially when the seeing is good. For a typical seeing of 0.″7, the motion of the telescope gives a round object an ellipticity of 0.2. After fitting ellipses to the H-band images, we fitted ellipses to the J and K images, keeping the shape of the isophotes constant. In this way radial color profiles could be determined. In Figure 1 we show $J-H$ and $H-K$ color profiles. In the figure, dotted lines indicate a radius corresponding to 1 seeing FWHM. Simulations have shown (e.g., Franx, Illingworth, & Heckman 1989; Peletier et al. 1990) that generally differences in seeing will not produce errors larger than 0.05 mag at radii larger than indicated by this line.

5. COMPARISON WITH THE LITERATURE

To check the quality of our photometry, we have made a number of comparisons with literature data. The surface brightness profiles in K were compared to the NIR array observations of McLeod & Rieke (1995) in K. The comparison is shown in Figure 2 and is good in general. In the central regions, our data tend to be brighter, due to our better seeing. In individual cases, however, this effect can be caused by variability in the luminosity of the AGN itself. Peterson et al. (1998), using an aperture of 5″ × 7.″6 characteristically find a variability in the optical continuum flux around 5000 Å of 10%–30% (rms). It appears that in the NIR, the amplitude of the variability is similar to that in the visual region. The origin of variability in the NIR apparently is heating of a dusty circumnuclear region by a variable nuclear source (Glass 1998 and references therein). The data in most cases show that this circumnuclear region has a temperature of about 1000–1300 K (Glass & Moorwood 1985; Alonso-Herrero et al. 1998), which implies that the variability in K is somewhat stronger than in H and J.

Somewhat further away from the center, between about 3″ and 10″ in radius, the difference between our results and those of McLeod & Rieke (1995) is generally constant as a function of radius. This means that the same surface bright-

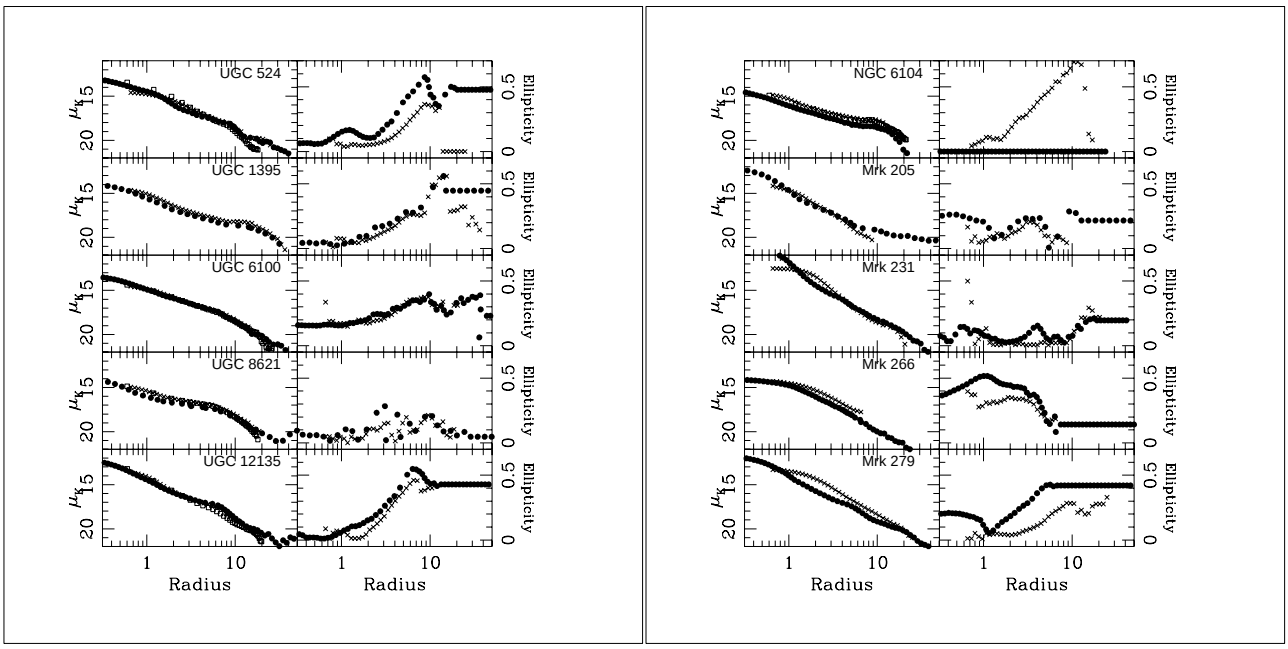

FIG. 2*a*

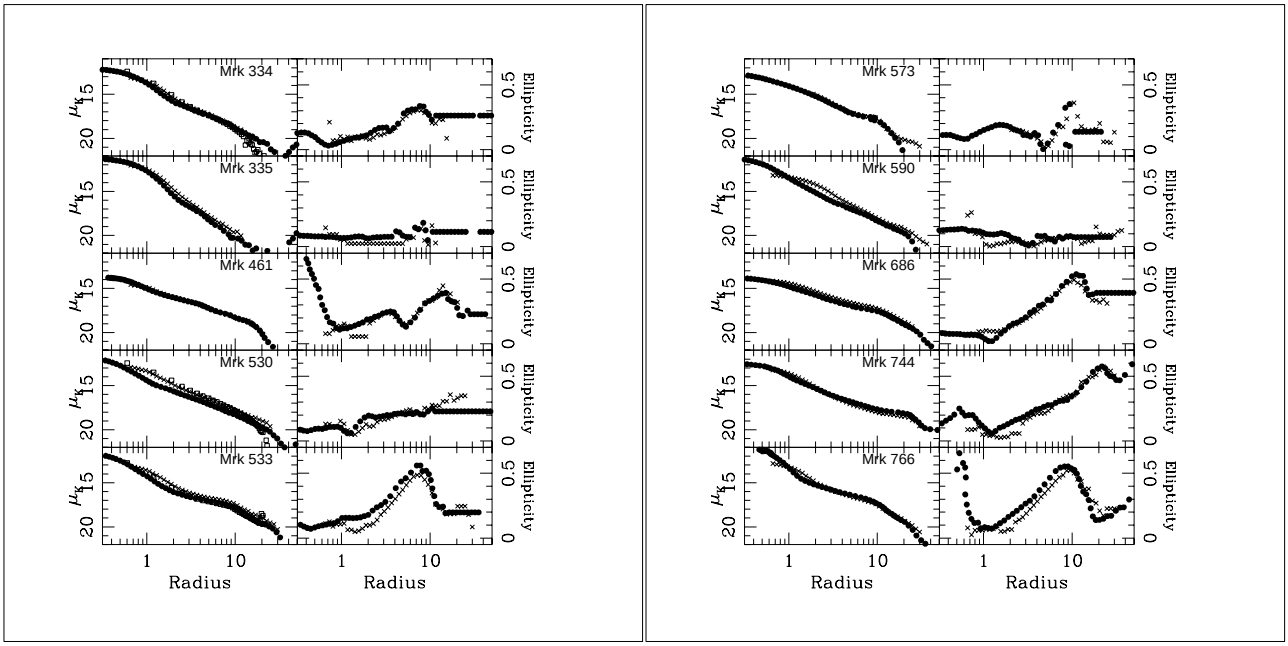

FIG. 2*b*

FIG. 2.—(*a*) Comparison with McLeod & Rieke (1995) and Hunt et al. (1997). Our data are indicated by filled circles. The data by McLeod & Rieke are indicated with crosses, and Hunt's data by open squares. (*b*) Comparison with McLeod & Rieke (1995) and Hunt et al. (1997). Our data are indicated by filled circles. The data by McLeod & Rieke are indicated with crosses, and Hunt's data by open squares. (*c*) Comparison with McLeod & Rieke (1995) and Hunt et al. (1997). Our data are indicated by filled circles. The data by McLeod & Rieke is indicated with crosses, and Hunt's data by open squares. (*d*) Comparison with McLeod & Rieke (1995) and Hunt et al. (1997). Our data are indicated by filled circles. The data by McLeod & Rieke are indicated with crosses, and Hunt's data by open squares.

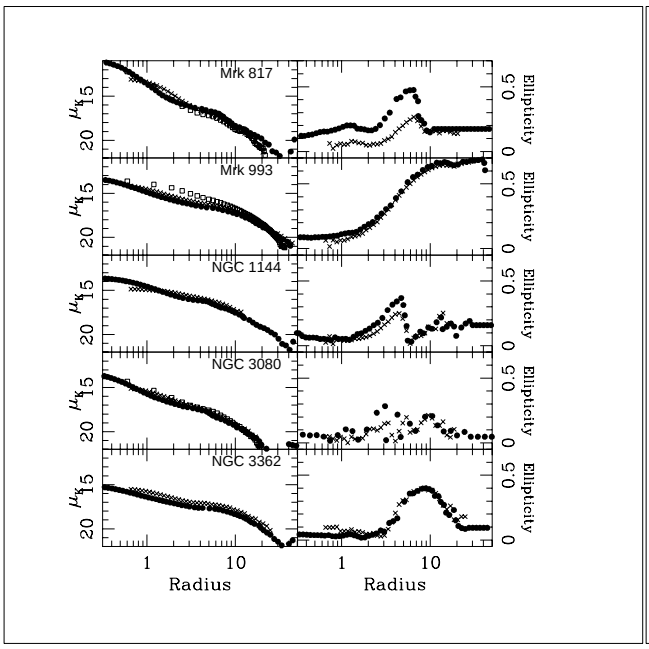
Mrk 817
Mrk 993
NGC 1144
NGC 3080
NGC 3362
Radius
Ellipticity

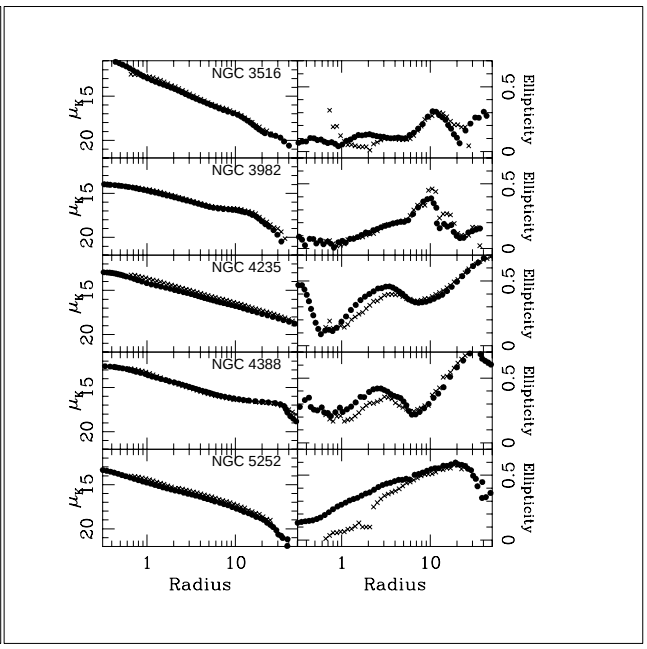
NGC 3516
NGC 3982
NGC 4235
NGC 4388
NGC 5252
Radius
Ellipticity

FIG. 2*c*

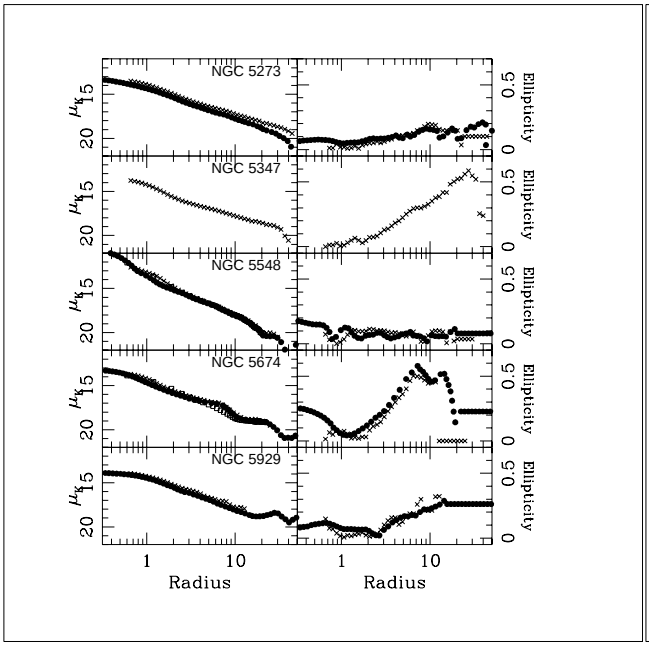
NGC 5273
NGC 5347
NGC 5548
NGC 5674
NGC 5929
Radius
Ellipticity

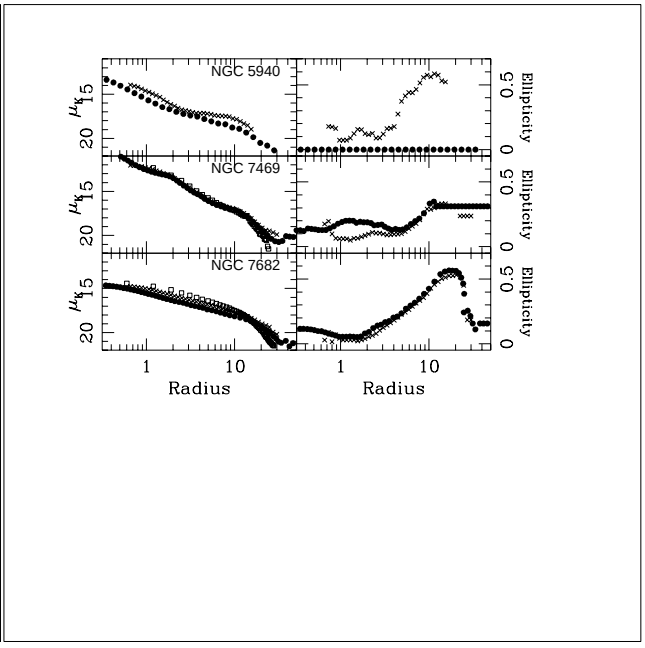
NGC 5940
NGC 7469
NGC 7682
Radius
Ellipticity

FIG. 2*d*

ness profile slope is measured, and hence the difference in surface brightness is caused by errors in the photometric calibration. The average offset between McLeod & Rieke and our results is 0.19 mag, with an rms scatter of 0.28 mag, implying that their data are slightly brighter. The agreement between the ellipticity profiles is good. Only near the center the profiles of McLeod & Rieke typically are rounder, generally due to seeing effects. For a few galaxies, we do not present an ellipticity profile. These galaxies are severely distorted, making it impossible to make unambiguous ellipse fits.

We compared the color profiles to the data of Hunt et al. (1997), where we have 15 galaxies in common. Apart from occasional differences of a few tenths of a magnitude in the color zero-point level, the $J-H$ and $H-K$ color profiles are very similar. Red features near the nucleus are always confirmed in the profiles of Hunt et al. (1997), except in a few cases, where the difference in seeing FWHM clearly affects their profiles.

Recently, Hunt et al. (1999) published an atlas with surface photometry of 90 Seyferts of type 1 and 2. For most of their galaxies they present infrared photometry in at least one band, while for many galaxies also optical photometry is presented. The median seeing of their infrared data is $\approx 1\farcs5$. Their ellipticity and position angle profiles are in reasonable agreement with the data published here. Comparing simulated aperture photometry for the 16 galaxies in common in apertures of 10″, 20″, and 30″ with the values presented in their Table 2, we find that our data are on the average, respectively, 0.09, 0.10, and 0.11 mag fainter, with a scatter of, respectively, 0.33, 0.31, and 0.31 mag, giving the same conclusion as our comparison with McLeod & Rieke (1995).

6. SUMMARY

In this paper, we have presented a subarcsec resolution J, H, and K imaging data set to study the properties of the host galaxies of Seyfert nuclei. It consist of images in the three bands of all but two galaxies of the CfA sample of Seyfert galaxies, a reasonably unbiased sample of nearby Seyfert 1's and 2's, and K-band images of a control sample, matched to the Seyfert sample, and observed to study morphological properties. The seeing and sampling is about a factor of 2 better than data published previously by McLeod & Rieke (1995). Here we provide for surface brightness and color profiles, ellipticity and major axis position angle profiles, including fits to the digital POSS survey, and gray-scale maps of surface brightness and both $J-H$ and $H-K$ colors. We have compared the color profiles with Hunt et al. (1997) for 15 galaxies in common, and the agreement is excellent. The comparison of the K-band surface brightness profiles with McLeod & Rieke (1995) also shows good agreement.

The data presented in this paper are analyzed in two companion papers. Knapen et al. (1999) and Shlosman et al. (1999), discuss bar properties and morphologies of Seyfert and normal hosts, address the issue of bar fraction in Seyferts and non-Seyferts, and focus on the color information presented here, in the framework of emission mechanisms in Seyfert 1's and 2's and in normal galaxies.

This paper is based in part on observations obtained at the William Herschel Telescope, which is operated at La Palma by the Isaac Newton Group in the Spanish Observatorio del Roque de los Muchachos of the Instituto de Astrofísica de Canarias. We thank Kim McLeod and Leslie Hunt for sending us their data tables. This research has made use of the NASA/IPAC Extragalactic Database (NED) which is operated by the Jet Propulsion Laboratory, California Institute of Technology, under contract with the National Aeronautics and Space Administration. Supported in part by NASA grants NAGW-3841 and WKU-522762-98-06, *HST* AR-07982.01-96A, and GO-08123.01-97A (I. S.). We used images from the Digitized Sky Survey, which was produced at the STScI under US Government grant NAG W-2166 and is based on photographic data obtained using Oschin Schmidt Telescope, operated by the California Institute of Technology and Palomar Observatory. We made use of observations made with the NASA/ESA *HST*, obtained from the data archive at STScI. STScI is operated by AURA, Inc., under NASA contract NAS 5-26555.

APPENDIX A

NOTES ON THE INDIVIDUAL OBJECTS

In this Appendix, we indicate specific features relevant to our study. We do not pretend to give a complete review of each object, or even to give up-to-date references for them. Most of the observations given here are directly based on our own images. In those cases where *HST* imaging is available from the *HST* archive, we have checked those images for relevant details and mention them where appropriate, again without pretending completeness. For some galaxies we have nothing to add to the knowledge already existing in the literature; we did, however, list those galaxies below in order to give the complete listing of our sample galaxies.

A1. CfA SAMPLE

Mrk 334.—Has some faint outer tails. *HST*: disturbed.

Mrk 335.—Compact appearance, except for a jetlike feature to the NW. *HST*: quasar-like.

UGC 524.—Face-on interacting spiral with outer arms.

1 Zw 1.—Irregular, point-source dominated object.

Mrk 993

Mrk 573.—Inner structure (inside 3″) possibly perpendicular to intermediate region ($<40''$), which in turn is perpendicular to an outer envelope, as visible on the POSS image.

UGC 1395

Mrk 590

NGC 1068.—Nearby AGN with strong bar, lens and tightly wound spiral arms.

NGC 1144
Mrk 1243.—Inner bar perpendicular to rest of galaxy.
NGC 3227.—Large nearby galaxy, closely interacting with NGC 3226.
NGC 3362.—Many spiral arms.
UGC 6100
NGC 3516.—Inner bar (at $\approx 10''$) in an outer envelope, very well visible on the POSS image.
Mrk 744.—Closely interacting with NGC 3788.
NGC 3982.—Circumnuclear SF.
NGC 4051.—Strong inner bar; irregular spiral arms, and fairly round in the outer parts.
NGC 4151.—Round bulge, with a strong outer bar. The very strong, red, central source makes the spikes of the telescope very well visible in the color maps. Some instrumental effects (ripples and low counts on one vertical semiaxis through the center) are visible as well.
NGC 4235
Mrk 766.—*HST*: bar.
Mrk 205.—Very close to NGC 4319, but with very different redshifts (0.07 for Mrk 205 vs. 0.006 for NGC 4319).
NGC 4388.—Dusty edge-on galaxy.
NGC 4395.—Nearby, low surface brightness dwarf galaxy, not observed in the NIR.
Mrk 231.—Irregular appearance. Faint tails in the outer parts seen on the POSS image and in de Robertis et al. (1998).
NGC 5033
Mrk 789.—Strongly interacting pair.
UGC 8621.—Three-armed spiral.
NGC 5252.—Featureless galaxy with slightly rounder outer regions. *HST*: polar ring.
Mrk 266.—Closely interacting pair.
Mrk 270.—Regular appearance. Has a small inner bar visible in the NIR.
NGC 5273
Mrk 461
NGC 5347.—Strongly barred galaxy, not observed in this paper.
Mrk 279.—The galaxy has a large, resolved red inner region, only visible in $H-K$.
NGC 5548.—Peculiar outer shells.
NGC 5674.—Face-on galaxy with a peculiar outer ring. The *HST* images show an inner bar perpendicular to the main bar.
Mrk 817.—*HST*: bar.
Mrk 686
Mrk 841.—Compact, point source dominated source.
NGC 5929.—Closely interacting with NGC 5930.
NGC 5940.—Strong bar in face-on galaxy. *HST*: bar.
NGC 6104.—Strong-barred, interacting system with shells. *HST*: bar.
UGC 12138.—Barred galaxy getting rounder in outer parts. *HST*: bar.
Mrk 335.—Compact appearance, except for a jetlike feature to the NW. *HST*: quasar-like.
NGC 7469.—Peculiar isophotes, interacting galaxy.
Mrk 530
Mrk 533.—Face-on spiral with a strong bar and a companion.
NGC 7682.—Strong bar in face-on galaxy. *HST*: bar.

A2. CONTROL SAMPLE

NGC 1093.—Strongly barred.
UGC 3247
UGC 3407.—Strongly barred galaxy, almost round in outer parts.
UGC 3463
UGC 3536.—Apparently edge-on, but outer regions getting round.
UGC 3576.—Outer regions much rounder than part visible on the NIR image.
UGC 3592.—Strongly barred, with bright star nearby.
NGC 2347
UGC 3789.—Strong-barred round, face-on galaxy.
NGC 2365
UGC 3850.—Galaxy has a large, round outer ring.
NGC 2431.—Inner bar perpendicular to rest of galaxy.
NGC 2460
NGC 2487.—Strongly barred round galaxy.
NGC 2599.—Large position angle twist.
NGC 2855
NGC 3066.—Strongly barred round galaxy.
NGC 3188.—Strongly barred round galaxy.
NGC 3455
NGC 4146

NGC 4369
NGC 4956
NGC 4966
NGC 5434.—Close companion of UGC 8967.
NGC 5534.—Very irregular appearance of an interacting galaxy.
NGC 5832.—Strong P.A. twist in the outer parts.
NGC 5869.—Ellipticity profile almost constantly rising.
UGC 9965.—Inner bar in round galaxy.
NGC 5992.—Face-on galaxy with wide spiral arms. Interacting with NGC 5993.
NGC 6085
NGC 6278
NGC 6504.—Edge-on.
NGC 6635
NGC 6922.—Peculiar spiral arms.

REFERENCES

Adams, T. F. 1977, ApJS, 33, 19
Alonso-Herrero, A., Simpson, C., Ward, M. J., & Wilson, A. S. 1998, ApJ, 495, 196
Antonucci, R. 1993, ARA&A, 31, 473
Athanassoula, E. 1996, in ASP Conf. Proc. 91, Barred Galaxies, ed. R. Buta, D. Crocker, & B. Elmegreen (San Francisco: ASP), 309
Balick, B., & Heckman, T. M. 1982, ARA&A, 20, 431
Barvainis, R. 1987, ApJ, 320, 537
Beckman, J. E., Peletier, R. F., Knapen, J. H., Corradi, R. L. M., & Gentet, L. J. 1996, ApJ, 467, 175
Bessell, M. S., & Brett, J. M. 1988, PASP, 100, 1134
Block, D., & Wainscoat, R. J. 1991, Nature, 353, 48
Carter, B. S., & Meadows, V. S. 1995, MNRAS, 276, 734
Dahari, O. 1984, Ph.D. thesis, Univ. California at Santa Cruz
de Robertis, M. M., Hayhoe, K., & Yee, H. K. C. 1998, ApJS, 496, 93
de Vaucouleurs, G., de Vaucouleurs, A., Corwin, H. G., Buta, R. J., Paturel, G., & Fouqué, P. 1991, Third Reference Catalog of Bright Galaxies (New York: Springer) (RC3)
Edelson, R. A., Malkan, M. A., & Rieke, G. H. 1987, ApJ, 323, 516
Franx, M., Illingworth, G., & Heckman, T. 1989, AJ, 98, 538
Fuentes-Williams, T., & Stocke, J. T. 1988, AJ, 96, 1235
Glass, I. 1998, MNRAS, 297, 18
Glass, I. S., & Moorwood, A. F. M. 1985, MNRAS, 214, 429
Heckman, T. 1978, PASP, 90, 241
Ho, L. C., Filippenko, A. V., & Sargent, W. L. W. 1996, ApJ, 487, 591
Huchra, J. P., & Burg, R. 1992, ApJ, 393, 90
Hughes, S. M., Roche, P., & Dhillon, V. S. 1996, WHIRCAM Users's Guide v1.0 (La Palma: Isaac Newton Group)
Hunt, L. K., Malkan, M. A., Rush, B., Bicay, M. D., Nelson, B. O., Stanga, R. M., & Webb, W. 1999, ApJS, in press
Hunt, L. K., Malkan, M. A., Salvati, M., Mandolesi, N., Palazzi, E., & Wade, R. 1997, ApJS, 108, 229
Jørgensen, I., Franx, M., & Kjaergaard, P. 1992, A&AS, 95, 489
Knapen, J. H., Shlosman, I., & Peletier, R. F. 1999, ApJ, in press (Paper II)
Lasker, B. M., Sturch, C. R., McLean, B. J., Russell, J. L., Jenkner, H., & Shara, M. M. 1990, AJ, 99, 2019
Malkan, M., Gorjian, V., & Tam, R. 1998, ApJS, 117, 25
McAlary, C. W. 1982, Ph.D. thesis, Univ. Toronto
McLeod, K. K., & Rieke, G. H. 1995, ApJ, 441, 96
Moles, M., Márquez, I., & Pérez, E. 1995, ApJ, 438, 604
Mulchaey, J. S., & Regan, M. W. 1997, ApJ, 482, L135
Mulchaey, J. S., Regan, M. W., & Kundu, A. 1997, ApJS, 110, 299
Nadeau, D., Murphy, D. C., Doyon, R., & Rowlands, N. 1994, PASP, 106, 909
Peletier, R. F. 1993, A&A, 271, 51
Peletier, R. F., & Balcells, M. 1997, New Astron., 1, 349
Peletier, R. F., Davies, R. L., Illingworth, G., Davis, L., & Cawson, M. 1990, AJ, 100, 1091
Peletier, R. F., Valentijn, E. A., Moorwood, A. F. M., Freudling, W., Knapen, J. H., & Beckman, J. E. 1995, A&A, 300, L1
Peterson, B. M., Wanders, I., Bertram, R., Hunley, J. F., Pogge, R. F., & Wagner, R. M. 1998, ApJ, 501, 82
Phinney, E. S. P. 1994, in Mass-Transfer Induced Activity in Galaxies, ed. I. Shlosman (Cambridge: Cambridge Univ. Press), 1
Rieke, G. H. 1978, ApJ, 226, 550
Rudy, R. J., Jones, B., Levan, P. D., Puetter, R. C., Smith, H. E., Willner, S. P., & Tokunaga, A. T. 1982, ApJ, 257, 570
Shlosman, I., Begelman, M. C., & Frank, J. 1990, Nature, 345, 679
Shlosman, I., Peletier, R. F., & Knapen, J. H. 1999, in preparation (Paper III)
Simkin, S. M., Su, H. J., & Schwarz, M. P. 1980, ApJ, 237, 404
Spillar, E. J., Oh, S. P., Johnson, P. E., & Wenz, M. 1992, AJ, 103, 793
Spinoglio, L., Malkan, M. A., Rush, B., Carrasco, L., & Recillas-Cruz, E. 1995, ApJ, 453, 616
Tadhunter, C., & Tsvetanov, Z. 1989, Nature, 341, 422
Thronson, H., Jr., et al. 1989, ApJ, 343, 158
Valentijn, E. A. 1990, Nature, 346, 153